Revista Brasileira de Ciência do Solo

Division – Soil Processes and Properties | Commission – Soil Physics

Stability of Soil Moisture Patterns Retrieved at Different Temporal Resolutions in a Tropical Watershed

Luís Romero Barbosa[(1)*], Nicholas Borges de Lira[(2)], Victor Hugo Rabelo Coelho[(3)], Alain Marie Bernard Passerat de Silans[(3)], André Nóbrega Gadêlha[(2)] and Cristiano das Neves Almeida[(3)]

[(1)] Institute of Environmental Science and Geography, University of Potsdam, Potsdam, BB 14476, Germany.
[(2)] Universidade Federal da Paraíba, Departamento de Engenharia Civil e Ambiental, Programa de Pós-Graduação em Engenharia Civil e Ambiental, João Pessoa, Paraíba, Brasil.
[(3)] Universidade Federal da Paraíba, Departamento de Engenharia Civil e Ambiental, João Pessoa, Paraíba, Brasil.

ABSTRACT: Above and underground hydrological processes depend on soil moisture (SM) variability, driven by different environmental factors that seldom are well-monitored, leading to a misunderstanding of soil water temporal patterns. This study investigated the stability of the SM temporal dynamics to different monitoring temporal resolutions around the border between two soil types in a tropical watershed. Four locations were instrumented in a small-scale watershed (5.84 km^2) within the tropical coast of Northeast Brazil, encompassing different soil types (*Espodossolo Humilúvico* or Carbic Podzol, and *Argissolo Vermelho-Amarelo* or Haplic Acrisol), land covers (Atlantic Forest, bush vegetation, and grassland) and topographies (flat and moderate slope). The SM was monitored at a temporal resolution of one hour along the 2013-2014 hydrological year and then resampled a resolutions of 6 h, 12 h, 1 day, 2 days, 4 days, 7 days, and 15 days. Descriptive statistics, temporal variability, time-stability ranking, and hierarchical clustering revealed uneven associations among SM time components. The results show that the time-invariant component ruled SM temporal variability over the time-varying parcel, either at high or low temporal resolutions. Time-steps longer than 2 days affected the mean statistical metrics of the SM time-variant parcel. Additionally, SM at downstream and upstream sites behaved differently, suggesting that the temporal mean was regulated by steady soil properties (slope, restrictive layer, and soil texture), whereas their temporal anomalies were driven by climate (rainfall) and hydrogeological (groundwater level) factors. Therefore, it is concluded that around the border between tropical soil types, the distinct behaviour of time-variant and time-invariant components of SM time series reflects different combinations of their soil properties.

Keywords: soil moisture variability, time-domain reflectometry, temporal resolution, Carbic Podzol, Haplic Acrisol.

*** Corresponding author:**
E-mail: luisromero.eng@gmail.com

Received: November 18, 2018
Approved: March 15, 2019

How to cite: Barbosa LR, Lira NB, Coelho VHR, Silans AMBP, Gadêlha AN, Almeida CN. Stability of soil moisture patterns retrieved at different temporal resolutions in a tropical watershed. Rev Bras Cienc Solo. 2019;43:e0180236.
https://doi.org/10.1590/18069657rbcs20180236

INTRODUCTION

Soil moisture (SM) is a crucial variable affecting biological, hydrological, and biogeochemical processes (Liu et al., 2010; Coppola et al., 2011; Rossato et al., 2013). However, the heterogeneous aspects of environmental factors convey an inherent high variability in time and space to SM, ranging from minutes to years and from centimetres to several kilometres (Vereecken et al., 2014). Some of the main factors driving SM variability are soil texture, vegetation, topography, and meteorological conditions (Mittelbach and Seneviratne, 2012; Liu et al., 2015), whose interactions trigger complex effects on SM time series (Zhu et al., 2014), which calls for a comprehensive analysis of its temporal stability and dynamics (Zhou et al., 2015). On this topic, an increasing number of studies have recently addressed new approaches to test SM spatiotemporal variability (Robinson et al., 2008). For example, Vereecken et al. (2014) have reviewed methods and techniques used to characterise SM at the field scale, including recent measurement advances such as remote sensing. Other studies have applied some of these techniques to analyse SM in small-, medium-, and large-scale watersheds under a wide variety of hydrological and climatic conditions (Vachaud et al., 1985; Qiu et al., 2001; Brocca et al., 2010; Souza et al., 2011; Molina et al., 2014; Zhu et al., 2014; Liu et al., 2015; Sun et al., 2015; Huang et al., 2016). Such analyses encompass techniques that hold copious applications that allow for revisiting the standard soil sampling schemes (Souza et al., 2011) and resetting the default monitoring time-step (Molina et al., 2014).

The SM stability concept, from a temporal perspective, was first introduced by Vachaud et al. (1985) to address time-invariant point-scale characteristics. The authors found a considerable time-stability in some locations, representing mean and extreme behaviours of SM throughout the year. Mittelbach and Seneviratne (2012) have decomposed a long-term SM time series between the temporal mean and temporal anomaly parcels to weigh the extent of that concept. Their results highlight the applicability of the invariant component in comparison to small contributions of the dynamic component to the overall variability. Conversely, other studies have found considerable implications of temporal anomalies on climate modelling (Viola et al., 2008), sub-seasonal forecasting (Weisheimer et al., 2011), land-atmosphere interactions (Hang et al., 2016), and satellite-derived product validations (Rötzer et al., 2015). The reliability of the stability concept is also intimately affected by the time-step of SM monitoring, because as the probe coverage footprint decreases, any monitoring disturbance tends to alter its mean integrated estimate. Molina et al. (2014) have claimed that a 10 × 10-m mesh grid (nine probes) would allow for estimating the mean time-stable SM in small homogeneous parcels. The authors reported no loss of information upon the daily SM variability by decreasing the 20-min temporal resolution to eight hours and one day during wetting-up and drying-down periods, respectively. In this context, temporal SM anomalies are of great interest in spatial variability analysis because they reduce the impacts of static soil properties on time series, although a considerable fraction of the spatial variability of these anomalies may be time-invariant (Mittelbach and Seneviratne, 2012; Brocca et al., 2014).

Despite the considerable number of SM spatiotemporal studies, some authors encourage further investigations over their time-variant and -invariant components worldwide due to the incipient knowledge on some ungauged regions (Mittelbach and Seneviratne, 2012). Brocca et al. (2014) have studied six different SM monitoring networks in distinct geographical regions and found that four featured standard deviation values of temporal anomalies lower than the standard deviation of raw SM data. Moreover, half of the addressed networks showed minimal spatial variability in moderate SM conditions when considering temporal anomalies. Souza et al. (2011) have applied the SM-relative differences ranking to identify sites in the Brazilian semi-arid that could reproduce the mean SM spatial pattern for agricultural water management purposes, while Silva Junior et al. (2016), Melo and Montenegro (2015), and Silva et al. (2015) have investigated the SM temporal dynamics and verified the importance of SM temporal stability studies for reducing

hydrological monitoring costs under different land cover and soil types. Concerning the impact of SM temporal dynamics, Costa et al. (2016) have investigated the permanence of soil water effectiveness under preserved-vegetation constraints in three semi-arid soil types. In a tropical volcanic archipelago, Montenegro et al. (2009, 2018) have investigated the water potential related to SM dynamics in three soil types to support local soil water management and conservation practices. Other relevant studies have also recently been carried out to assess the influence of SM dynamics on sedimentological processes (e.g. Montenegro and Ragab, 2010; Montenegro et al., 2013; Figueiredo et al., 2016). Table 1 provides a tabular chronological literature review of relevant studies on SM dynamics, also describing the advancements on the SM time-stability method.

All studies listed in table 1 have been carried out using the SM time-stability method applied in distinct areas throughout the world, at different spatiotemporal resolutions and with various methods of analysis. Nevertheless, Brocca et al. (2017) point out the scarcity of SM data available in the International Soil Moisture Network: relevant data are mostly from the USA and Europe. In Brazil, studies about spatiotemporal stability methods still prompt an insufficient understanding of regional SM heterogeneities in this continental-scale country, not allowing for extending conclusions of previous investigations to other particular soil types. Furthermore, the studies listed in table 1 provide insights into the effects of different temporal resolutions of monitoring over time-variant and -invariant components by neglecting the influences of SM peaks and recession mischaracterisation on the statistical metrics that summarise its temporal variability/stability. It is hypothesised that comparing the mean statistical metrics of the SM time-variant and time-invariant components at different temporal resolutions may allow for pointing out the temporal stability of soil water patterns.

Against this background, this study aimed to investigate the stability of the SM temporal dynamics (Mittelbach and Seneviratne, 2012) to different monitoring temporal resolutions (such as Molina et al., 2014) around the border between two soil types in a tropical watershed. For this purpose, the SM time series of four monitoring locations were assessed at eight temporal resolutions to identify how their time-variant and time-invariant parcels prompt SM temporal variability among sites with different soil types (*Espodossolo Humilúvico* or Carbic Podzol, and *Argissolo Vermelho-Amarelo* or Haplic Acrisol), land covers (Atlantic Forest, bush vegetation, and grassland) and topographic (flat and moderately sloped) features. The present study revisits and employs a framework of statistical metrics recently updated (Mittelbach and Seneviratne, 2012) for analysing the SM temporal dynamics on a point-scale basis, around a low-density and poorly-monitored tropical area with well-distinguished rainy and dry seasons.

MATERIALS AND METHODS

Study area

The study was carried out at the Guaraíra Experimental Watershed (GEW) on the tropical coast of Northeast Brazil (Figure 1). The watershed covers 5.84 km^2 between the coordinates 7° 32'-7° 27' S and 34° 04'-35° 02' W. Since 2003, it has been operated and monitored by the Hydrology Network of Semi-Arid (REHISA), which is currently composed of eight federal universities in Brazil (Montenegro and Ragab, 2010; Coelho et al., 2017). The monitoring program set to this experimental watershed makes an important experimental contribution to Brazilian hydrology, since the GEW is strategically located near the transition zone between the Atlantic Forest (tropical climate) and *Caatinga* (semi-arid climate) biomes, in a coastal sedimentary area, where the largest cities in tropical Northeast Brazil are located. Its natural vegetation encompasses a mix of *Capoeira* (secondary-growth bush vegetation) and Atlantic Forest remnants; part of this native vegetation was also cleared for cultivating sugarcane and pineapple crops (Sales et al., 2014).

Table 1. Summary of relevant literature on soil moisture spatiotemporal variability using different methods and spatiotemporal resolutions

Study	Location/climate/study size	Temporal resolution/ time length/device	Main soil moisture analyses and methods
Vachaud et al. (1985)	(i) Grenoble, France; (ii) Seville, Spain and (iii) Mornag, Tunisia/(i) n.r.; (ii) n.r.; (iii) n.r. / (i) 2 km^2; (ii) n.r.; (iii) 0.01 km^2	(i) 14 days and bimonthly; (ii) n.r.; and (iii) n.r./(i) 2.5 years; (ii) n.r.; and (iii) n.r./(i) neutron tubes; (ii) neutron tubes and tensiometers; and (iii) neutron tubes and gravimetric method	Introduced the concept of soil moisture time-stability and variability in order to reduce the number of soil sample observations
Qiu et al. (2001)	Losses Plateau, China/Continental semi-arid/3.5 km^2	Biweekly/9 months/TDR	Used the metrics proposed by Vachaud et al. (1985), associated with the local features (climate, soil type, and elevation), in order to reduce the number of local soil moisture measurements
Brocca et al. (2010)	Vallaccia catchment, central Italy/Mediterranean semi-humid/56 km^2	35 sampling days with almost weekly frequency, except for the summer period/1 year/TDR	Applied the methodology proposed by Vachaud et al. (1985) in distinct sites inside the catchment to define the minimal number of measurement points to validate soil moisture data provided by remote sensing products
Souza et al. (2011)	Mimoso catchment, North-Eastern Brazil/Semi-Arid very hot/1,800 m^2	Twice per week/96 days/ neutron tubes	Evaluated the soil moisture time-stability concept proposed by Vachaud et al. (1985) and its dependence in an irrigated carrot plot
Brocca et al. (2012)	Genna and Caina catchments, central Italy/Mediterranean semi-humid/242 and 178 km^2, respectively	35 and 34 sampling days with almost weekly frequency, respectively, except for the summer period/11 months/TDR	Applied the methodology proposed by Vachaud et al. (1985) at small and medium spatial scales in order to reduce the number of measuring points across the region
Mittelbach and Seneviratne (2012)	14 grassland sites in Switzerland/Six distinct climates/~31,500 km^2	Daily/14 months/TDR and capacitance	Updated the method proposed by Vachaud et al. (1985), using a framework to distinguish the time-variant and -invariant contributors to spatial variability at country scale
Brocca et al. (2014)	Italy, Spain, France, Switzerland, Australia, and United States/Distinct climates/From 250 to 150,000 km^2	From daily to 15 days/ From 10 months to less than 3.5 years/n.r.	Compared the framework carried out by Mittelbach and Seneviratne (2012) with soil moisture data and the saturation percentage in six monitoring networks worldwide
Molina et al. (2014)	Can Vila catchment, Northeast Spain/Mediterranean humid/0.56 km^2	From 20 minutes to 14 days/2 years/TDR	Evaluated how distinct monitoring temporal resolutions can impact the spatiotemporal changing patterns in order to define the most appropriated monitoring frequency under distinct soil moisture conditions
Melo and Montenegro (2015)	Jatobá experimental watershed, Northeast Brazil/ Semi-arid very hot/14 km²	16 biweekly campaigns in 18 monitoring points/1.25 years/Neutron tubes	Investigated the soil moisture temporal variability in surface and sub-surface layers under Caatinga vegetation and pasture cover in *Argissolo Amarelo* (Haplic Acrisol) and *Neossolo Regolítico* (Dystric Regosol) soil types
Silva Junior et al. (2016)	Jatobá experimental watershed, Northeast Brazil/ Semi-arid very hot/14 km²	42 campaigns in 17 monitoring points with n.r. frequency/3.5 years/ capacitance probe	Evaluated surface soil moisture temporal stability under Caatinga vegetation and pasture cover to identify stable points in *Argissolo Amarelo* (Haplic Acrisol) and *Neossolo Regolítico* (Dystric Regosol) soil types
Costa et al. (2016)	Aiuaba experimental watershed, Northeast Brazil/ Semi-arid very hot/12 km²	Hourly/8 years/TDR	Estimated the permanence curves for soil moisture and water effectiveness in *Argissolo Eutrófico* (Haplic Lixisol), *Luvissolo Crômico* (Chromic Luvisol), and *Neossolo Litólico* (Lithic Leptsol) soil types
Montenegro et al. (2018)	Experimental plot in Fernando de Noronha archipelago, Northeast Brazil/Tropical with dry summer/49.5 m²	Hourly/2 years/TDR	Investigated the relationship between soil water temporal dynamics and rainfall patterns and rainfall erosivity in a *Cambissolo Háplico* (Sodic Cambisol)
This study	Guaraíra experimental watershed, Northeast Brazil/Tropical with dry summer/5.84 km^2	From 1 hour to 15 days/1 year/TDR	Evaluated how different monitoring temporal resolutions (Molina et al., 2014) can affect the time-variant and -invariant soil moisture components (Mittelbach and Seneviratne, 2012) around the border between *Espodossolo Humilúvico* (Carbic Podzol) and *Argissolo Vermelho-Amarelo* (Haplic Acrisol) soil types

n.r. = not reported.

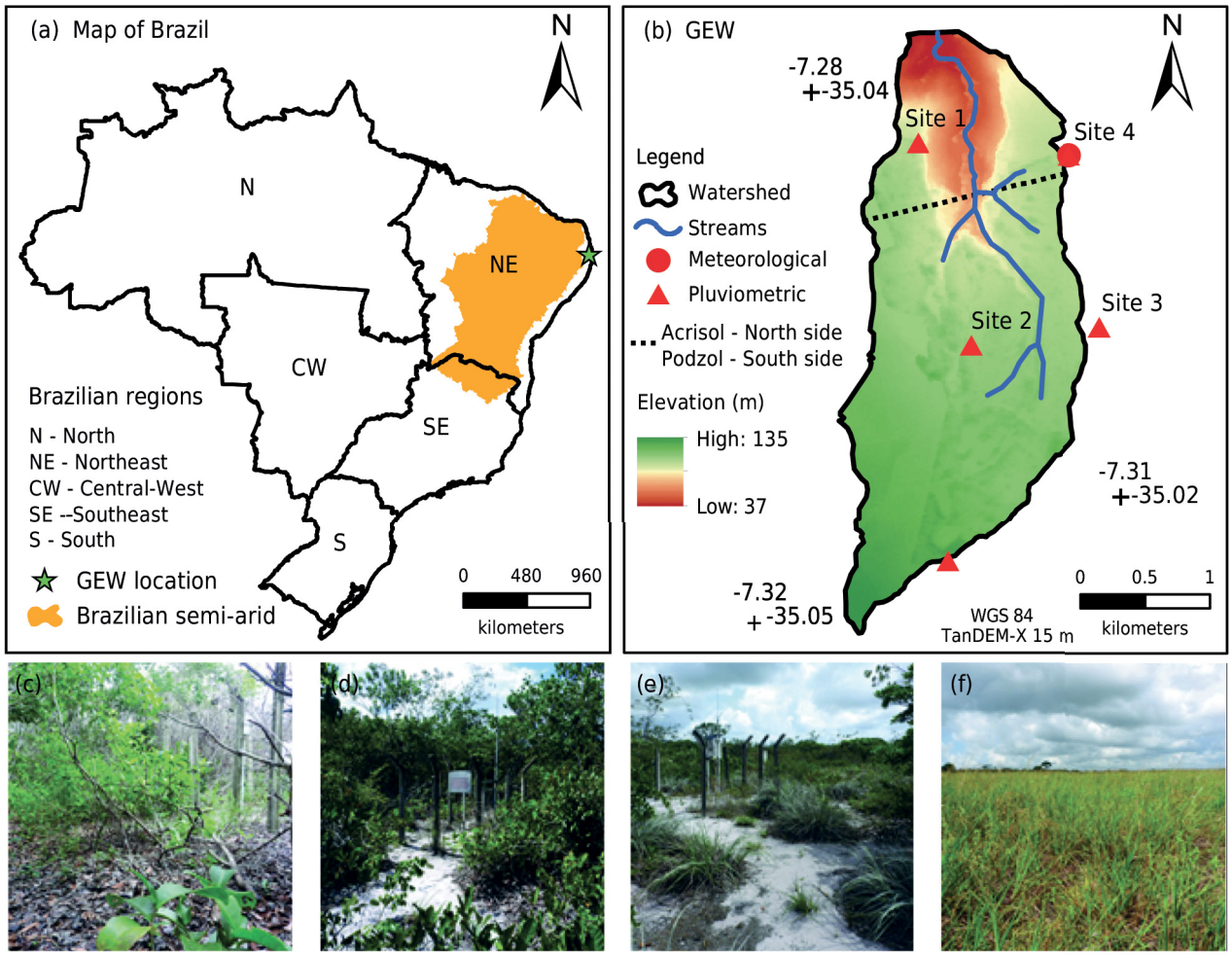

Figure 1. Study area in Northeast Brazil (a) and the four sampling sites in the Guaraíra Experimental Watershed (b): site 1 (c), site 2 (d), site 3 (e), and site 4 (f).

According to Köppen's climate classification system (Köppen, 1936), analysed in detail across Brazil by Alvares et al. (2013), the region holds a tropical climate with a dry summer (As), whose mean temperature is around 26 °C. Mean annual rainfall is ~1,700 mm, most of which (~70 %) occurs from March to July, i.e. in autumn-winter seasons (Barbosa et al., 2018). Accordingly, mean annual class-A pan evaporation reaches ~1,300 mm in the GEW (Silva et al., 2000). Its elevation ranges from 37 to 135 m above mean sea level, and its mean slope rate is 1.8 %, being more sloped at downstream and flat at upstream. Quaternary-age sediments, originating from regional basement erosion, cover the study area. Two soil types are present in the GEW: Carbic Podzol and Haplic Acrisol, according to the World Reference Base (WBR) for soil resources (IUSS Working Group WRB, 2015) (Figure 1b). These soils are equivalents to *Espodossolo Humilúvico Hidromórfico dúrico-arênico* and *Argissolo Vermelho-Amarelo Distrófico típico*, according to the Brazilian Soil Classification System (SiBCS), respectively (Santos et al., 2018). *Argissolo* (Acrisol) holds a thick layer with deep well-drained soil, while *Espodossolo* (Podzol) presents an illuvial silica-cemented restrictive layer at a depth of ~2 m (MA and SUDENE, 1972). These features confer to the study area a complex underground system characterized by thickness alternations of the vadose zone, varying from thin to thick.

Near-surface SM measurements were registered at four fixed sites located within the GEW, monitoring rainfall (sites 1, 2, and 3) and meteorological data (site 4). The meteorological data available at site 4 were as follows: relative air humidity, soil heat flux, soil and air temperature, net radiation, and wind speed. The physical properties of each site are shown in table 2.

Table 2. Physical properties of the studied sites in the Guaraíra Experimental Watershed (GEW), Brazil

Site	Vegetation cover	Soil type	Coarse sand[(1)]	Fine sand[(1)]	Silt and clay[(1)]	Soil texture	Bulk density	Slope
			g kg^{-1}				Mg m^{-3}	
1	Atlantic Forest	Haplic Acrisol[(2)]	416	564	20	Sand	1.23	Moderately sloped
2	Atlantic Forest	Carbic Podzol[(3)]	503	481	16	Sand	1.26	Flat
3	Bush vegetation	Carbic Podzol[(3)]	503	483	14	Sand	1.36	Flat
4	Grassland	Haplic Acrisol[(2)]	400	570	30	Sand	1.32	Flat

[(1)] Soil particle size distribution obtained by sieving essay. [(2)] *Argissolo Vermelho-Amarelo*. [(3)] *Espodossolo Humilúvico*.

Soil moisture monitoring and temporal resolutions

Time-Domain Reflectometry (TDR) probes (CS616, Campbell Scientific) were installed, calibrated, and automatically monitored the SM of each site at one-hour temporal resolution. The TDR probes were vertically inserted to indirectly represent the integrated mean of SM along the first 0.30 m below the surface. The SM data were assimilated from April 2013 to April 2014, throughout the hydrological year. The original time-step of monitoring was then used as the reference scenario for this study.

Seven SM scenarios were investigated with increasingly coarser temporal resolutions of six h, 12 h, 1 day, 2 days, 4 days, 7 days and 15 days. Coarser temporal resolutions were obtained from the one-hour reference scenario by excluding the intermediary registers, e.g. the six-hour temporal resolution was obtained by ignoring the five previous hourly values. This procedure was the same as that used by Molina et al. (2014), hypothesising that the intermediate records are not available for the excluded time scales. The new temporal series were analysed and compared independently for each analysis described in the following sections.

Soil moisture and its time-variant and time-invariant components

In this study, S represents the SM, while time and space are termed *t* and *n*, respectively. Therefore, S_{tn} indicates the SM at t and n. The variables *T* and *N* denote the total number of time registers and sites (four sites), respectively.

Similar to Mittelbach and Seneviratne (2012), the SM temporal mean is termed as M_{tn}, the time-invariant component, whereas the SM temporal anomaly as A_{tn}, the time-variant component. Thus, the relation between them is defined by equation 1:

$$S_{tn} = M_{tn} + A_{tn} \quad \text{Eq. 1}$$

The SM variability and stability in time at any site were studied in the GEW through the combination of classical approaches (Vachaud et al., 1985) and improvements (Brocca et al., 2012; Mittelbach and Seneviratne, 2012; Brocca et al., 2014). Accordingly, the same notations used by Mittelbach and Seneviratne (2012) and Brocca et al. (2014) for the mean (μ) and standard deviation (σ) were replicated in this study. Then, equations 2 and 3 show the temporal mean $\mu_{\hat{t}}(S_{tn})$ and the temporal standard deviation $\sigma_{\hat{t}}(S_{tn})$ at any site in the GEW, where the subscript $\hat{t}$ was used for indicating the temporal statistic meaning, as follows:

$$\mu_{\hat{t}}(S_{tn}) = M_{tn} = \frac{1}{T}\sum_{t=1}^{T}(S_{tn}) \quad \text{Eq. 2}$$

$$\sigma_{\hat{t}}(S_{tn}) = \sqrt{\frac{1}{T}\sum_{t=1}^{T}[S_{tn} - \mu_{\hat{t}}(S_{tn})]^2} \quad \text{Eq. 3}$$

The absolute values of A_{tn}, $|A_{tn}|$ were used to circumvent compensation between positive and negative values in the statistical metrics. Subsequently, equation 4 shows their temporal mean $\mu_t(|A_{tn}|)$, as follows:

$$\mu_t(|A_{tn}|) = \frac{1}{T}\sum_{t=1}^{T} |A_{tn}| \quad \text{Eq. 4}$$

Furthermore, equation 5 shows the SM spatial mean $\mu_n(S_{tn})$ at any time, calculated as the arithmetic mean of S_{tn} among the four sites. Similarly, equation 6 shows the $|A_{tn}|$ spatial mean $\mu_n(|A_{tn}|)$ at any time, calculated as the arithmetic mean of $|A_{tn}|$ among the four sites. The subscript n (without ^) was used here to indicate that this spatial mean does not represent the mean value within an area, but a mean value of spatially different sites:

$$\mu_n(S_{tn}) = \frac{1}{N}\sum_{n=1}^{N} S_{tn},\ N = 4 \quad \text{Eq. 5}$$

$$\mu_n(|A_{tn}|) = \frac{1}{N}\sum_{n=1}^{N} |A_{tn}|,\ N = 4 \quad \text{Eq. 6}$$

Time-stability ranking upon the absolute and relative differences of time-variant and time-invariant components

The time-stability concept proposed by Vachaud et al. (1985) was adopted to identify the more representative sites to the SM spatial mean within a network. The notations Δ and δ, adopted by Vachaud et al. (1985) and Mittelbach and Seneviratne (2012), were used to represent the absolute and relative differences, respectively. Accordingly, the symbol ΔS_{tn} is defined as the absolute difference between S_{tn} and the SM spatial mean $\mu_n(S_{tn})$, as shown in equation 7:

$$\Delta S_{tn} = S_{tn} - \mu_n(S_{tn}) \quad \text{Eq. 7}$$

Equations 8 and 9 show how the ΔS_{tn} temporal mean $\mu_t(\Delta S_{tn})$ and the standard deviation $\sigma_t(\Delta S_{tn})$ are calculated:

$$\mu_t(\Delta S_{tn}) = \frac{1}{T}\sum_{t=1}^{T} \Delta S_{tn} \quad \text{Eq. 8}$$

$$\sigma_t(\Delta S_{tn}) = \sqrt{\frac{1}{T}\sum_{t=1}^{T} [\Delta S_{tn} - \mu_t(\Delta S_{tn})]^2} \quad \text{Eq. 9}$$

Equations 10, 11, and 12 show how the relative difference δS_{tn} and its temporal mean $\mu_t(\delta S_{tn})$ and standard deviation $\sigma_t(\delta S_{tn})$ are calculated:

$$\delta S_{tn} = \frac{\Delta S_{tn}}{\mu_n(S_{tn})} \quad \text{Eq. 10}$$

$$\mu_t(\delta S_{tn}) = \frac{1}{T}\sum_{t=1}^{T} \delta S_{tn} \quad \text{Eq. 11}$$

$$\sigma_t(\delta S_{tn}) = \sqrt{\frac{1}{T}\sum_{t=1}^{T} [\delta S_{tn} - \mu_t(\delta S_{tn})]^2} \quad \text{Eq. 12}$$

Time-stability ranking was performed over the metrics obtained at different temporal resolutions for the four monitored sites, ordering their respective deviation from the overall mean. As such, the $\mu_t(\Delta S_{tn})$ and $\mu_t(\delta S_{tn})$ from each monitored site in the GEW were arranged from the smallest to the largest. The closest points to $\mu_n(S_{tn})$, i.e. sites with

$\mu_t(\delta S_{tn})$ and $\mu_t(\Delta S_{tn})$ near zero, were then considered the most stable. Additionally, the structure proposed by Vachaud et al. (1985) and adapted by Mittelbach and Seneviratne (2012), which considers the absolute terms $|\Delta S_{tn}|$ and $|\delta S_{tn}|$, was also adopted. Their means and standard deviations were then similarly obtained and arranged in ascending order by their respective means, i.e. $|\mu_t(\Delta S_{tn})|$ and $|\mu_t(\delta S_{tn})|$.

The time-stability analyses carried out according to equation 7 to equation 12 can be extended through equation 1 to include the different components of absolute SM, as previously applied by Mittelbach and Seneviratne (2012). The absolute values of these components are used because A_{tn} may have negative values. Consequently, the following equations are used:

$$|\Delta A_{tn}| = |A_{tn} - \mu_n(A_{tn})| \quad \text{Eq. 13}$$

$$|\Delta M_{tn}| = |M_{tn} - \mu_n(M_{tn})| \quad \text{Eq. 14}$$

The temporal means and standard deviations of the absolute anomalies, i.e. $\mu_t(|\Delta A_{tn}|)$ and $\sigma_t(|\Delta A_{tn}|)$, were ranked according to their respective deviation from the overall mean. Similarly, the absolute variation of the temporal mean ΔM_{tn} results, i.e. $\mu_t(|\Delta M_{tn}|)$, were also ranked. Lastly, comparison between the ranking of the temporal mean of absolute SM differences ($|\mu_t(\Delta S_{tn})|$) and its decomposed parts ($|\mu_t(\Delta M_{tn})|$ and $|\mu_t(\Delta A_{tn})|$), obtained at different temporal resolutions, was performed, which allow for inferring on how the time-variant and -invariant components (Vachaud et al., 1985) incorporate the SM temporal dynamics at different sites.

Descriptive statistics and hierarchical clustering

The descriptive statistics of the SM datasets at each site n and time t (S_{tn}), namely, the mean, standard deviation, coefficient of variation, minimum and maximum values, were calculated for every preselected temporal resolution: the reference scenario and the others seven scenarios (see section 2.2). Box plots were also drawn representing mean, median, quartiles (25 and 75 %), quantiles (10 and 90 %), and outliers (less than 10 %- and higher than 90 %-quantiles). Based on this, it was possible to identify how data losses may affect the temporal behaviour of the time series as well as which sites are more sensitive to a decrease in temporal resolution.

Hierarchical cluster analysis was also applied to the main time-variant and time-invariant components of the SM, i.e. S_{tn}, ΔS_{tn}, δS_{tn}, A_{tn}, ΔA_{tn}, M_{tn}, and ΔM_{tn}, to assess the association between these variables. This analysis was used to compare how the dendrograms changed from site to site and within each site, considering different temporal resolutions. The Euclidean distance measure (Deza and Deza, 2009) and Ward's method (Ward Jr, 1963) were used to link the dendrograms. As different variables with unequal ranges were used in this study, the first step of the clustering comprised the procedure of standardisation, so that all of them ranged from -1 to 1. This standardisation was carried out through the mean and standard deviation of each variable dataset. Subsequently, pairwise distances were calculated using the Euclidean distance, termed as D_{link}. The maximum distance was estimated between variables, termed as D_{max}. This study used the relative Euclidian distance D_{link}/D_{max} (in percentage) to link the SM components and to enable comparison between different sites and different temporal resolutions at the same site.

RESULTS

Temporal analysis of absolute soil moisture

Approximately 30,000 SM measurements at one-hour temporal resolution were processed at each analysed site in the GEW throughout the study year 2013/2014. Some sites exhibited a lack of data throughout this period, which represents ~12 % of the total

dataset. The accumulated rainfall over the area was 1,942 mm in this hydrological year, ~12 % higher than the mean long-term rainfall. Due to these forcing events, the SM time series displayed successive peaks and recessions throughout the hydrological year, in which the sites 2 and 3 featured greater and smaller amplitudes, respectively (Figure 2). Rainfall events registered from June to September 2013 led to noticeable SM increases, whose values at all sites ranged from 8.1 (site 3) to 114.6 mm (site 2) for these months. The minimum SM values for *Espodossolo Humilúvico* (Carbic Podzol) were 5.6 (site 2) and 6.5 mm (site 3), whereas at *Argissolo Vermelho-Amarelo* (Haplic Acrisol), the values were 8.4 (site 1) and 12.2 mm (site 4). The SM temporal pattern during the summer dry season (from October 2013 to January 2014) presented maximum values up to 54.6 mm when all sites were considered.

The descriptive statistics of SM, used to analyse time periods according to the temporal resolutions in this study, is shown in table 3. Noticeably, since the temporal resolution is longer, the mean, standard deviation and coefficient of variation of SM values slightly increase. Regarding the SM maximum values, changes are more perceptible, decreasing from 33 to 42 % between temporal resolutions of one hour and 15 days at sites 1 and 4, respectively. Relevant changes in the maximum values of these two specific cases were observed between temporal resolutions of 12 hours and 1 day. Although more noticeable at sites 1 and 4, such decreasing behaviour implies some substantial loss of information also at site 2 with coarsening of the temporal resolution. However, although site 2 presented a higher peak oscillation (Figure 2), data losses were irrelevant for the temporal mean. On the other hand, non-extensive data losses were registered at site 3 due to its slow SM recession.

Figure 3 presents the box plots of SM for every monitored site and all temporal resolutions analysed in this study. Visually, at all sites, the distance between the mean and median in the box plot remained unchanged in the scenarios when temporal resolution of sampling increased from 1 hour to 15 days. Accordingly, the intervals between the 25 and 75 % quartiles were not notably modified among the analysed temporal resolutions, which means that, visually, the frequency distributions were unchanged along the scenarios. On the other hand, the main changes between the different temporal resolutions are the substantial reduction of outliers below and above the extreme quantiles (i.e. 10 and 90 %, respectively) at all sites. This behaviour indicates that the SM dynamics are no longer correctly represented when the temporal resolution reduces. The losses of maximum and minimum values, as the temporal resolution increases, portray the inaccurate assimilation of the SM dynamics at coarser temporal resolutions.

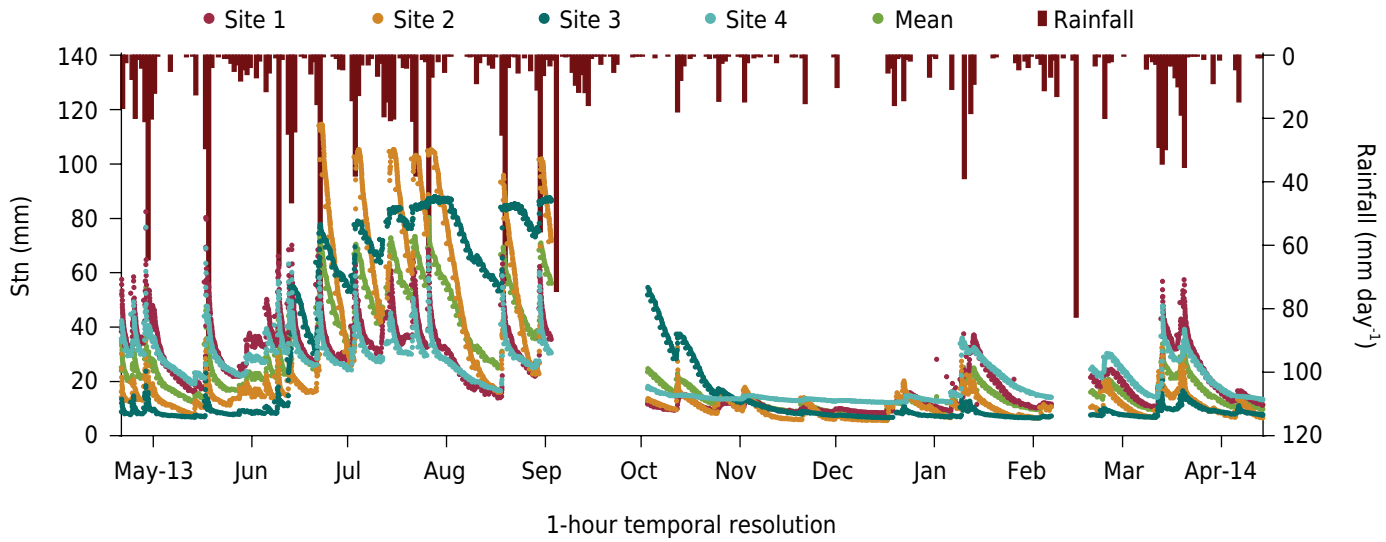

Figure 2. Hourly soil moisture (St_n) and daily rainfall in the Guaraíra Experimental Watershed (GEW), Brazil.

Table 3. Soil moisture descriptive statistics per site and temporal resolution

Site	Temporal resolution	Mean	Standard deviation	Coefficient of variation	Minimum	Maximum
			mm	%	mm	
1	1 hour	22.71	12.70	56.91	8.40	82.47
	6 hours	22.73	12.81	56.35	8.40	76.38
	12 hours	22.81	12.88	56.46	8.40	70.15
	1 day	22.35	12.13	54.28	8.40	56.61
	2 days	22.25	11.91	53.53	8.49	56.61
	4 days	22.61	12.35	54.62	8.58	51.77
	7 days	23.57	13.45	57.07	8.49	55.52
	15 days	23.36	13.67	58.53	8.86	55.52
2	1 hour	23.36	25.71	110.10	5.61	114.61
	6 hours	23.41	25.79	110.14	5.61	114.49
	12 hours	23.46	25.76	109.79	5.66	114.25
	1 day	23.04	25.57	110.99	5.66	114.13
	2 days	22.86	25.59	111.96	5.71	114.13
	4 days	23.16	26.00	112.26	5.75	104.84
	7 days	25.75	29.87	115.99	5.71	104.62
	15 days	23.66	27.98	118.25	6.04	101.90
3	1 hour	26.68	28.23	105.80	6.51	88.00
	6 hours	26.72	28.27	105.80	6.54	87.86
	12 hours	26.77	28.33	105.84	6.55	87.58
	1 day	26.55	28.26	106.44	6.55	87.17
	2 days	26.35	28.16	106.85	6.58	87.17
	4 days	26.06	28.12	107.92	6.94	86.89
	7 days	27.46	29.62	107.89	6.55	87.17
	15 days	25.60	28.70	112.09	6.55	84.26
4	1 hour	22.78	9.00	39.52	12.21	76.78
	6 hours	22.81	9.11	39.93	12.21	65.73
	12 hours	22.85	9.16	40.10	12.21	63.53
	1 day	22.45	8.47	37.71	12.21	45.10
	2 days	22.41	8.30	37.03	12.21	44.09
	4 days	22.70	8.59	37.83	12.21	41.39
	7 days	23.17	9.48	40.90	12.29	44.19
	15 days	23.39	9.41	40.21	12.29	44.19

Temporal variability analysis of time-variant and time-invariant components

Figure 4 shows the SM variability by depicting the temporal means of time-invariant (M_{tn}) and absolute time-variant [$\mu_t(|A_{tn}|)$] components at each site. Site 3 presented the highest M_{tn}, whereas sites 1 and 4 showed the smallest ones; similar values (below 23 mm) were noticed at temporal resolutions varying from 1 hour to 4 days (Figure 4a). It is worth noting the increase in M_{tn} at sites 2 and 3 at a temporal resolution of 7 days, with a value above 27 mm at site 3. In addition, site 2 showed an M_{tn} between 22 and 24 mm, but displayed a critical increase (near 26 mm) at 7 days. The M_{tn} values at all sites were closer to the spatial-temporal mean [$\mu_n(M_{tn})$] at a temporal resolution of 15 days, except for site 3. The increase of M_{tn} at 7 days, at both sites 2 and 3, can be explained by losses of minimum SM data in areas where the soil is saturated for long periods (Figure 2). On the other hand, the observed SMC reduction at 15 days can be explained by losses

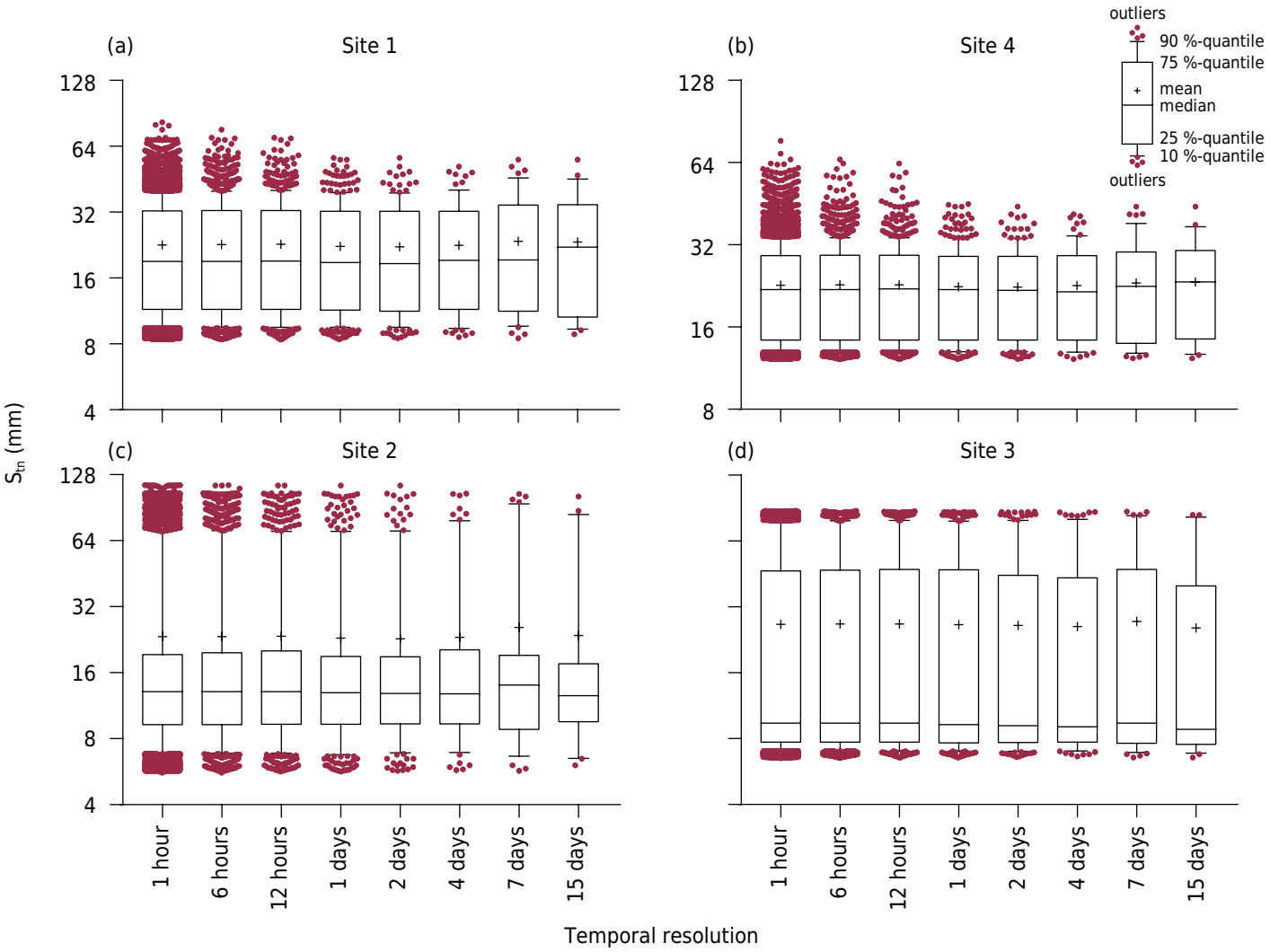

Figure 3. Soil moisture box plots per site and temporal resolution.

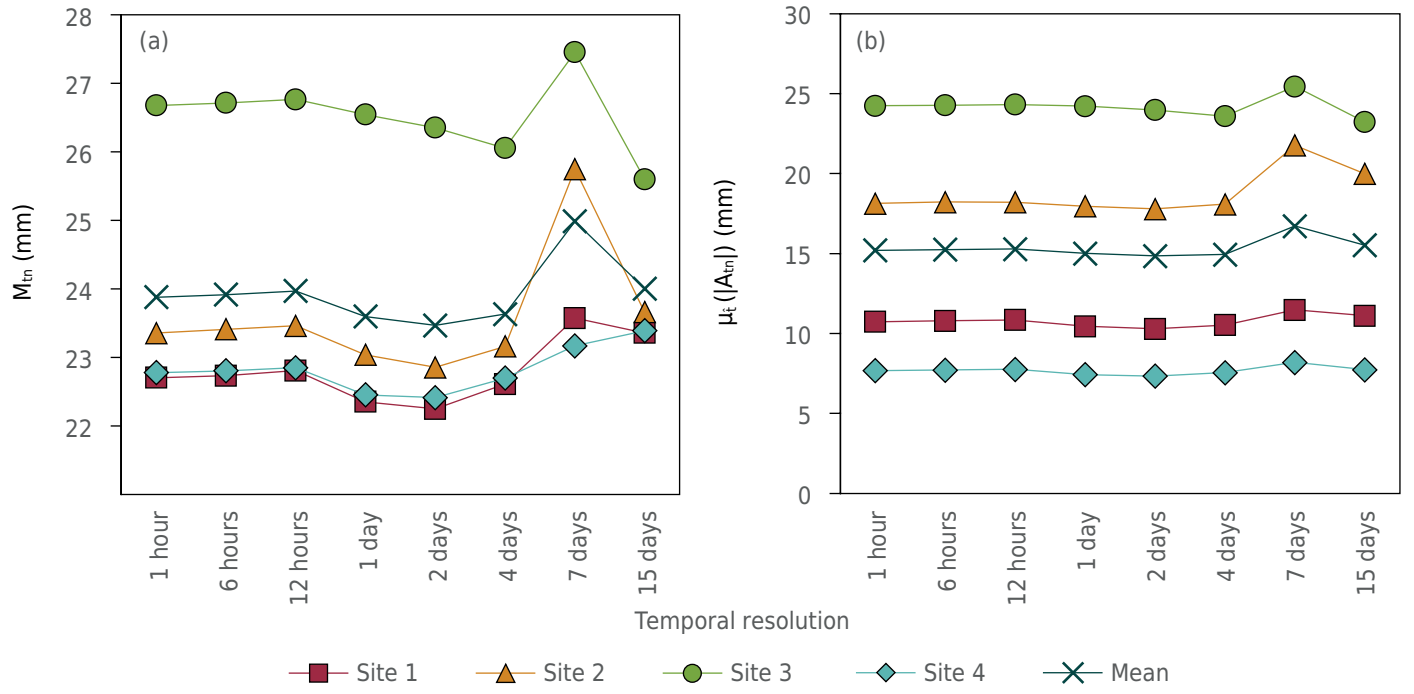

Figure 4. Temporal variability of the temporal mean of (a) time-invariant (M_{tn}) and (b) time-variant [$\mu_t(|A_{tn}|)$] values per site and temporal resolution.

of maximum SMC data. These contrasted behaviours, from temporal resolutions of 4 to 15 days, compromise and mischaracterise the SM in the GEW when coarser temporal resolutions of monitoring are set at the sites 2 and 3.

The temporal anomalies were considered as absolute values ($|A_{tn}|$) in figure 4b to circumvent compensations among positive and negative values. It was possible to observe A_{tn} changes at different temporal resolutions, although they were less perceptible than those in temporal mean (M_{tn}) cases. However, both plots showed a similar behaviour, namely unusual high values at 7-day temporal resolution. This result stemmed from data losses caused by temporal resolution decreases in the time series, which had a stronger effect on the spatial mean of the SM temporal mean [$\mu_n(M_{tn})$] than on the spatial mean of the absolute temporal anomalies [$\mu_n(|A_{tn}|)$]. The invariant term was then more sensitive than the variant one. Therefore, SM time-stability was slightly spatially affected by temporal anomalies (A_{tn}) in the GEW, since the temporal mean of the absolute temporal anomalies [$\mu_t(|A_{tn}|)$] remained roughly unchanged at all sites.

Analyses of rank stability changing at different temporal resolutions

Rank stability was performed to analyse and compare the absolute and relative differences of the SM components at different temporal resolutions at all sites (Figures 5, 6, and 7). However, only the results for the temporal resolutions at which the site ranking changed from 1-hour temporal resolution were displayed due to the large amount of data used in this analysis. The temporal resolutions of 4, 7, and 15 days were then plotted together with the 1-hour reference scenario because the temporal resolutions ranging from 6 h to 2 days remained unchanged when compared to the original scenario.

Figure 5 shows the ranking stability plots of the calculated and absolute temporal means of absolute SM differences [$\mu_t(\Delta S_{tn})$ and $|\mu_t(\Delta S_{tn})|$, respectively] and of relative SM differences [$\mu_t(\delta S_{tn})$ and $|\mu_t(\delta S_{tn})|$, respectively]. At first, it is possible to notice that $\mu_t(\delta S_{tn})$ rankings remain the same at all analysed temporal resolutions. Additionally, sites 2 and 4 showed an SM temporal variability closer to the mean behaviour at absolute scale, because their $\mu_t(\Delta S_{tn})$ values were closest to zero at almost all temporal resolutions. On the other hand, sites 3 and 1 were closer to the mean behaviour at relative scale, since the $\mu_t(\delta S_{tn})$ values were nearly zero. Likewise, the 4-days temporal resolution revealed a double swapping of rank positions for $|\mu_t(\delta S_{tn})|$ between sites 1 and 3 and sites 2 and 4 (Figures 5m and 5n), remaining the same at 7-day and 15-day temporal resolutions (Figures 5o and 5p). Such consideration also took place for $\mu_t(\Delta S_{tn})$ and $|\mu_t(\Delta S_{tn})|$ at 7 days, which alternated the rank positions between sites 1 and 4 at 1st and 2nd and 2nd and 3rd ranks, respectively (Figures 5c and 5g). Despite the change in rank positions between the two first non-reference temporal resolutions (from 4 to 7 days), the ranking of the sites for $\mu_t(\Delta S_{tn})$ and $|\mu_t(\Delta S_{tn})|$ returned to the original setting at 15-day temporal resolution. These behaviours upheld the SM data losses at coarser temporal resolutions at sites 1, 2, and 4, but not at site 3. Therefore, the rank positions of most sites were sensitive to data losses entailed by reducing the temporal resolution, leading to ranking mischaracterisation.

Figure 6 shows the rank stability plots of the temporal means of the absolute SM temporal means and the absolute anomaly differences [the $\mu_t(|\Delta M_{tn}|)$ and $\mu_t(|\Delta A_{tn}|)$, respectively]. Importantly, the $\mu_t(|\Delta M_{tn}|)$ ranking had the same order than the $|\mu_t(\Delta S_{tn})|$ ranking (Figures 5e to 5h and 6a to 6d). Site 2 was the most representative in terms of the SM spatial mean within the monitoring network for all temporal resolutions, while site 3 was the least representative site (Figures 6a to 6d), even holding a similar soil type and prolonged recession curves. Furthermore, the $\mu_t(|\Delta M_{tn}|)$ tended to decrease as the temporal resolution became coarser, except at the 7-day temporal resolution, when almost all sites (1, 2, and 4) presented an opposite tendency. Thus, the longer the temporal resolution of data collection, the smaller the $\mu_t(|\Delta M_{tn}|)$ magnitudes, since the SM time series become more susceptible to anomalies in A_{tn}. As such, the sites tend to decrease their amplitudes in

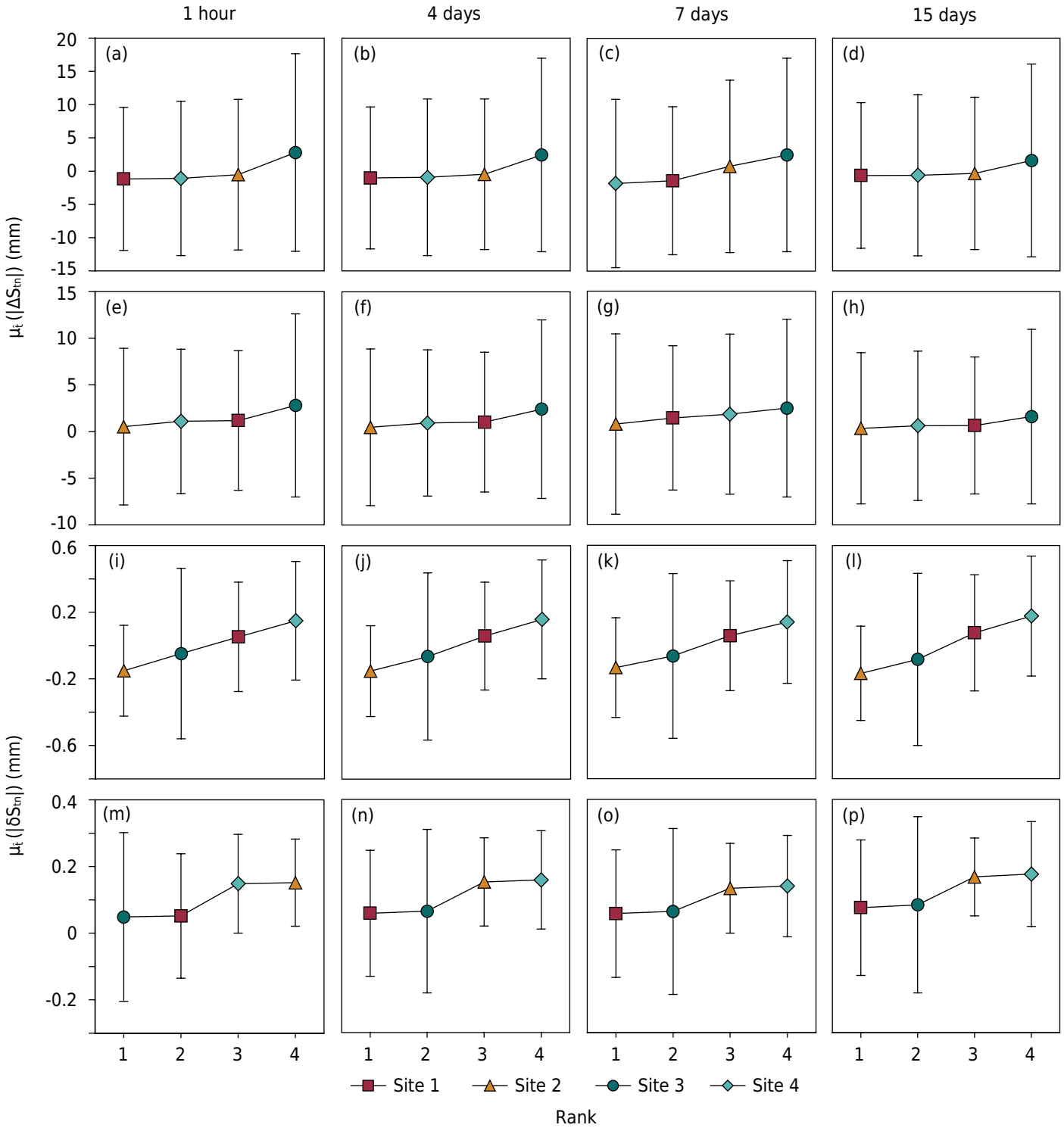

Figure 5. Ranking stability plots of temporal means of absolute Soil Moisture (SM) differences [$\mu_t(\Delta S_{tn})$] (a, b, c, and d), absolute temporal means of absolute SM differences [$|\mu_t(\Delta S_{tn})|$] (e, f, g), and temporal means of relative SM differences [$\mu_t(\delta S_{tn})$] and absolute temporal means of relative SM differences [$|\mu_t(\delta S_{tn})|$] (i, j, k, and l).

different proportions, depending on the soil features, which may trigger an alteration in the ranking. The ranks of $\mu_t(|\Delta M_{tn}|)$ and $\mu_t(|\Delta A_{tn}|)$ swapped positions between sites 1 and 4 (Figures 6a and 6c) and between sites 1 and 2 (Figures 6f and 6g) at 7-day temporal resolution, respectively. This result corroborates with those results ascertained in the descriptive statistical analysis (see section 4.1). Therefore, the results suggest that the real SM processes are mischaracterised at a temporal resolution of 7 days, since the ranking of their temporal components changed in comparison to the reference scenario; the mentioned temporal resolutions show magnitudes higher than those in the reference scenario.

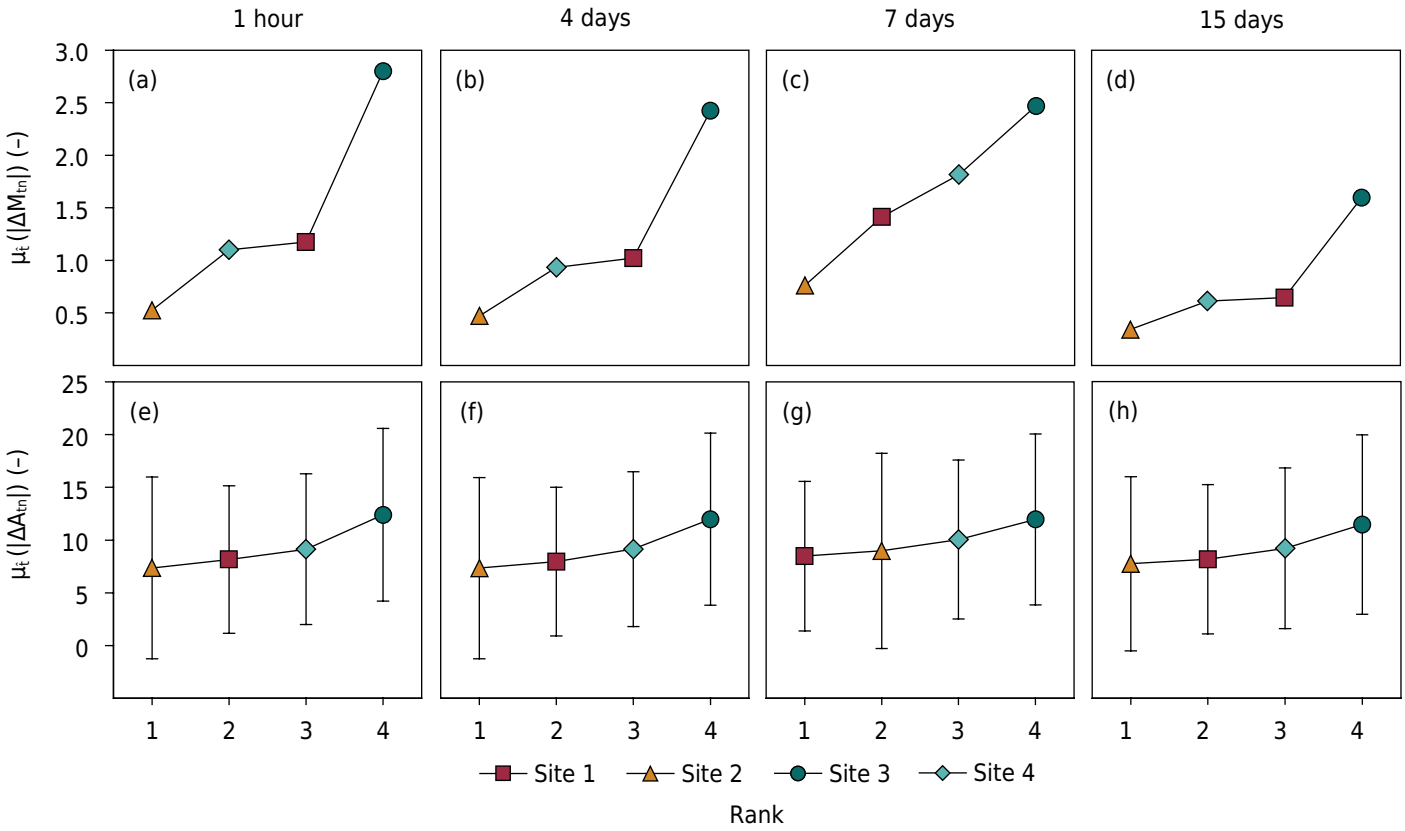

Figure 6. Ranking stability plots of temporal means of absolute soil moisture temporal mean differences [$\mu_t(|\Delta M_{tn}|)$] (a, b, c, and d) and temporal means of absolute temporal anomaly differences [$\mu_t(|\Delta A_{tn}|)$] (e, f, g, and h).

Figure 7 shows the scatter plots of the ranking of the absolute temporal means of absolute SM differences [$|\mu_t(\Delta S_{tn})|$] against the rankings of $\mu_t(|\Delta M_{tn}|)$ and $\mu_t(|\Delta A_{tn}|)$. Sites 2 and 3 presented the lower and higher ranks for both relationships, respectively, without relevant variations (only site 2 in figure 7g) by changing the temporal resolutions. Conversely, sites 1 and 4 presented different ranks in the relationship of $|\mu_t(\Delta S_{tn})|$ against $\mu_t(|\Delta M_{tn}|)$ and $|\mu_t(\Delta S_{tn})|$ against $\mu_t(|\Delta A_{tn}|$. It is highlighted that the ranking of the study sites has the same relationship between $|\mu_t(\Delta S_{tn})|$ and $|\mu_t(\Delta M_{tn})|$ for all analysed temporal resolutions, meaning that sites 1 and 4 swapped their ranks between the 2nd and 3rd positions in both metrics (Figure 7c). On the other hand, alternations in the ranks of $|\mu_t(\Delta S_{tn})|$ and $\mu_t(|\Delta A_{tn}|)$ were observed at a temporal resolution of 7 days, where sites 1 and 2 swapped their 2nd and 1st positions in $|\mu_t(\Delta S_{tn})|$, respectively, and sites 4 and 1 swapped their 2nd and 3rd positions in $\mu_t(|\Delta A_{tn}|)$, respectively (Figure 7g). Accordingly, the results presented in this analysis show that the invariant mean parcel mainly rules the SM variability.

Hierarchical cluster analysis

Hierarchical cluster analysis was carried out for all study sites by using the SM temporal components for all considered temporal resolutions. However, no relevant cluster reordering was found by changing the analysis for temporal resolutions longer than 1 hour, since a nearly stable and robust cluster association was found between SM components at all sites. Accordingly, the dendrogram for all study sites, using SM temporal components at 1-hour temporal resolution, is shown in figure 8. Overall, sites 1 and 4 had similar dendrograms, which is likely substantiated by the similarity of their soil type, land covers and topographic features (Figure 1). On the other hand, the dendrograms of sites 2 and 3 were similar, likely influenced by the *Espodossolo* (Podzol) flat areas and land covers (sparse Atlantic Forest and bush vegetation), which have a sandy texture in the first soil horizon (high permeability) and a restrictive layer nearby at a depth of ~2 m.

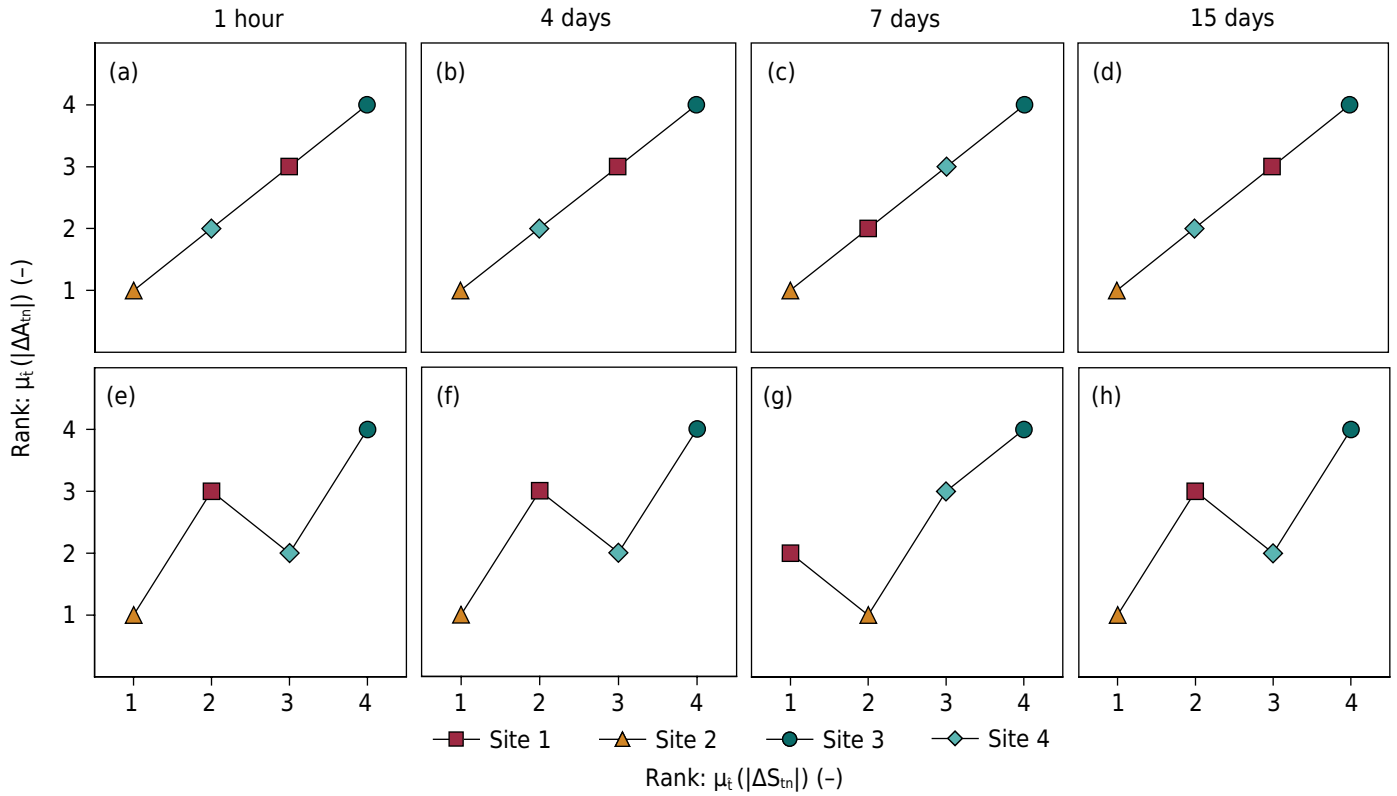

Figure 7. Scatter plots of absolute temporal mean ranking of absolute soil moisture differences [$|\mu_t(\Delta S_{tn})|$] against the temporal mean ranking of absolute SM temporal mean differences $\mu_t(|\Delta M_{tn}|)$ (a, b, c, and d) and temporal mean ranking of absolute temporal anomaly differences $\mu_t(|\Delta A_{tn}|)$ (e, f, g, and h).

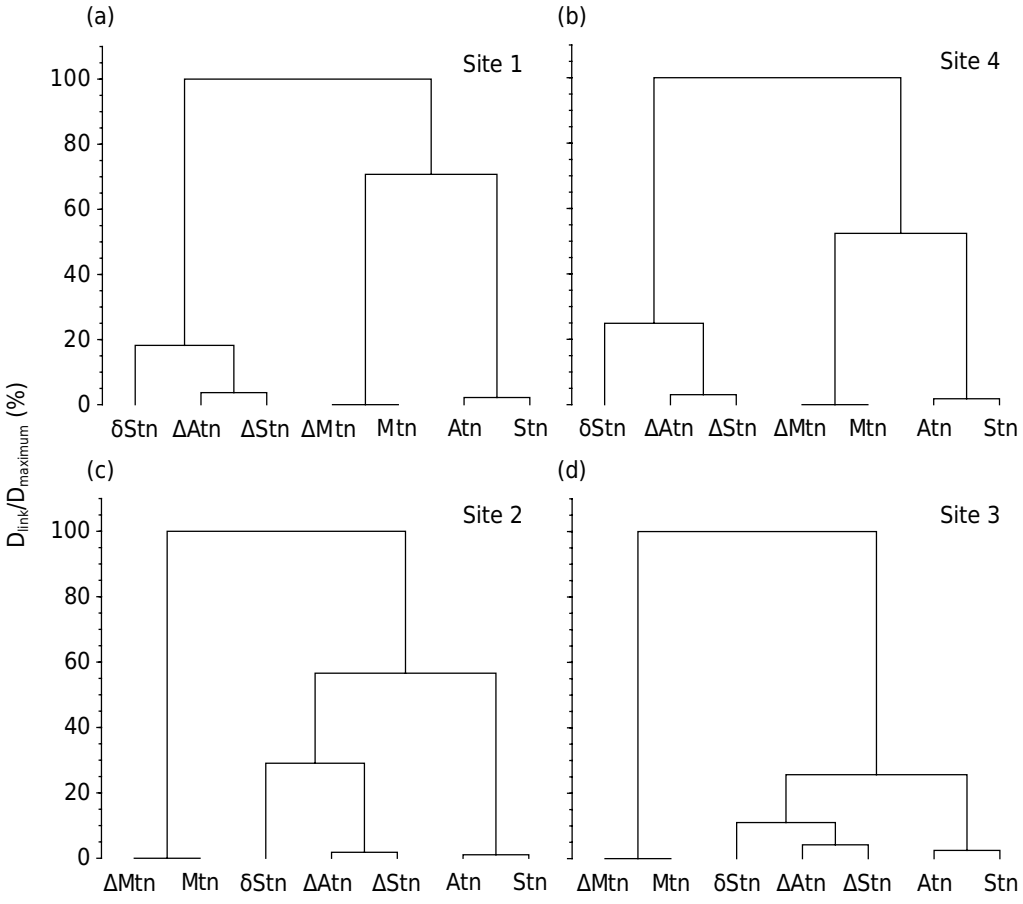

Figure 8. Dendrogram of the main temporal soil moisture components at 1-hour temporal resolution at site 1 (a), site 4 (b), site 2 (c), and site 3 (d), according to the Euclidean distance dissimilarity measure and Ward's cluster method.

Based on the hierarchical clustering, it can be inferred that S_{tn} and A_{tn} had fast links at all sites. The relative D_{link}/D_{max} for these two variables ranged from 1 to 3 %, mainly due to the influence of the dynamic parcel on the SM behaviour. This linkage reinforces that temporal anomaly is the primary SMC component reflecting the temporal variability patterns, irrespective of land cover, soil type and slope (Figure 1). A similar linkage was found between variables ΔS_{tn} and ΔA_{tn}, with D_{link}/D_{max} varying from 2 to 5 %, followed by δS_{tn} values ranging from 11 to 29 %. This behaviour denotes the reasonable influence of the dynamic parcel ample oscillation on the magnitude of SM temporal variability. On the other hand, M_{tn} and ΔM_{tn} seemed to link belatedly to S_{tn} and A_{tn} at sites 1 and 4, with D_{link}/D_{max} varying from 52 to 71 %, respectively; however, they were completely separated at sites 2 and 3 (D_{link}/D_{max} equals 100 %). This result corroborates with previous findings of this study, showing the negligible SM time-variant effects over the overall time-invariant aspect of SM dynamics at the downstream sites of GEW compared to the upstream ones.

DISCUSSION

Soil moisture (SM) temporal dynamics at downstream behaved differently from the upstream of the border between two tropical soil types, similar to the findings reported in small-scale watersheds by Dias et al. (2015) and Hu et al. (2017), but not to the results of other studies (Qiu et al., 2001; Zhou et al., 2015). Ranking rearrangements at 7 days were incited by some weekly rainfall peaks, associated with prolonged soil saturation events during the rainy season (mainly at sites 2 and 3), which led to losses of minimum values (Figure 6), whose effects have also been reported by Zhang and Shao (2017). Moreover, the slight decrease in $\mu_t(|\Delta M_{tn}|)$ at site 3 was likely imposed by non-processing the high SMC peaks at coarser temporal resolutions, since high values with slow recession curves are more frequent during the wet season at this site (Figure 2), which has also been found by Molina et al. (2014).

The reason the SM time series at sites 1 and 4 show smaller amplitudes despite the sandy soil texture is that these sites feature either a moderately sloped topography or the absence of a shallow restrictive layer, characteristic of *Argissolo Vermelho-Amarelo* (Haplic Acrisol). These properties increase the water residence time in the *Argissolo* (Acrisol), yielding a deeper groundwater recharge, similar to Amazon *Espodossolo* (Podzol)-to-*Argissolo* (Acrisol) soil transition (Nascimento et al., 2008). The sandy texture in *Argissolo Vermelho-Amarelo* (Haplic Acrisol) is in agreement with the GEW hydrodynamic characterisation (Santos et al., 2012), but differs from the overall *Argissolo* (Acrisol) texture elsewhere (Montenegro and Ragab, 2012; Ottoni et al., 2018). This combination of soil properties demonstrates the particular condition of the study area.

Around the border between the two soil types, site 2 is a representative spot in the middle of the GEW, mainly because is better represented both the SM temporal variability (Figure 5) and its invariant and dynamic parcels at the reference scenario (Figure 6). The high peaks and the quick recession curves stem from the capillarity rise effect due to the shallow groundwater table, which comes close to saturation during the rainy season (Figure 2), as previously described by Montenegro et al. (2018) in *Cambissolo Háplico* (Sodic Cambisol). Still, at upstream of the border between the two soil types, the waterlogging lasted longer at site 3 because of its proximity to the watershed boundary, where the groundwater is shallower. These behaviours typically occur in thin, flat soil packages associated with restrictive layers (duripan in this study), because they hold a high water permanence subjected to sub-surface percolation processes (Costa et al., 2016).

Although sites 2 and 3 showed the highest maximum SM peaks along the rainy season, they also showed the lowest SM values during the dry season. The slightly higher SM in the dry season at downstream is likely related to the presence of mulch (Souza et al.,

2011). The minimum SM values for *Espodossolo Humilúvico* (Carbic Podzol) and *Argissolo Vermelho-Amarelo* (Haplic Acrisol) soil type plots (Table 3) were higher than those obtained by Costa et al. (2016) for *Argissolo Eutrófico* (Haplic Lixisol), *Luvissolo Crômico* (Chromic Luvisol) or *Neossolo Litólico* (Lithic Leptsol) in the same region. Most likely, this is because coastal watersheds are susceptible to a tropical regime with high rainfall rates in the rainy season, differently from the Caatinga biome over a very hot semi-arid zone (Barbosa et al., 2018; Rozante et al., 2018; Gadelha et al., 2019), where 70 % of the SM drop below the wilting point (Costa et al., 2016).

Therefore, SM temporal variability was mainly ruled by its invariant mean parcel (Figures 7a to 7d), which was mainly affected by steady soil properties (soil type and slope), as reported in different areas worldwide (Mittelbach and Seneviratne, 2012; Rosenbaum et al., 2012; Zhao et al., 2013; Brocca et al., 2014; Hu et al., 2017; Brocca et al., 2017). On the other hand, the time-variant parcel had a small influence on SM temporal variability, which was controlled mainly by climatic (rainfall) and hydrogeological (groundwater level) factors (Figures 7e to 7h) (Mittelbach and Seneviratne, 2012; Neris et al., 2012; Li and Rodell, 2013; Zhao et al., 2013; Brocca et al., 2014; Hirschi et al., 2014; Vereecken et al., 2014; Brocca et al., 2017). Conversely, the land cover conditions had a lower seasonal influence on SM temporal dynamics, which has also been reported by Melo and Montenegro (2015) in *Argissolo Amarelo* (Haplic Acrisol) and *Neossolo Regolítico* (Dystric Regosol).

CONCLUSIONS

The present study demonstrated that varying the soil moisture (SM) monitoring time-step at some sites and ranking the mean statistical metrics of their SM time-variant and time-invariant parcels may point out changes on the stability of SM temporal dynamics. It is concluded that around the border between tropical soil types, the distinct behaviours of time-variant and time-invariant components of SM time series reflect the different combinations of their soil properties, namely topographic slope, depth to the restrictive layer, and soil texture. Moreover, the steady soil properties over time, such as slope and soil type, regulate the SM temporal mean, whereas the variable properties in time, such as rainfall events and groundwater table, control the SM temporal dynamics. The rearrangements in site rankings mainly stem from differences in the time-invariant parcel, which govern SM temporal variability over the time-variant parcel, either at high or low temporal resolutions. Lastly, losses of SM monitoring resolution mainly affect the SM time-variant parcel, hinting at the potential mischaracterisation of the SM time-stability in tropical soil types for time-steps longer than 2 days.

ACKNOWLEDGMENTS

The authors would like to acknowledge the financial support from the Brazilian Innovation Agency (FINEP) granted to the BRAMAR (Brazil Managed Aquifer Recharge, project's grant number: 557/2013. This study was partly funded by the Coordenação de Aperfeiçoamento de Pessoal de Nível Superior - Brasil (CAPES) - Finance Code 001. The first/corresponding author holds a scholarship granted by CAPES within the Programa Conjunto de Bolsas de Doutorado na República Federal da Alemanha - 2017/2018 - Process No. 88887.161412/2017-00, between CAPES/CNPq (Conselho Nacional de Desenvolvimento Científico e Tecnológico - Brasil)/DAAD (Deutscher Akademischer Austauschdienst). In addition, the authors also acknowledge the CNPq and the Fundação de Apoio à Pesquisa do Estado da Paraíba - Brasil (FAPESQ) for research (PQ, PDJ and DTI-B) and postgraduate (PhD and Master) scholarships. The authors also acknowledge the thoughtful inputs of the anonymous reviewers, which undoubtedly contributed to improve the quality of the paper.

AUTHOR CONTRIBUTIONS

Conceptualization: Nicholas Borges de Lira, Alain Marie Bernard Passerat de Silans, and Cristiano das Neves Almeida.

Methodology: Luís Romero Barbosa, Nicholas Borges de Lira, Alain Marie Bernard Passerat de Silans, and Cristiano das Neves Almeida.

Formal analysis: Luís Romero Barbosa, Nicholas Borges de Lira, Victor Hugo Rabelo Coelho, André Nóbrega Gadêlha, and Cristiano das Neves Almeida.

Investigation: Luís Romero Barbosa, Nicholas Borges de Lira, Alain Marie Bernard Passerat de Silans, and Cristiano das Neves Almeida.

Writing – original draft preparation: Luís Romero Barbosa, Nicholas Borges de Lira, and Victor Hugo Rabelo Coelho.

Writing – review and editing: Luís Romero Barbosa, Victor Hugo Rabelo Coelho, Alain Marie Bernard Passerat de Silans, André Nóbrega Gadêlha, and Cristiano das Neves Almeida.

REFERENCES

Alvares CA, Stape JL, Sentelhas PC, Gonçalves JLM, Sparovek G. Köppen's climate classification map for Brazil. Meteorol Z. 2013;22:711-28. https://doi.org/10.1127/0941-2948/2013/0507

Barbosa LR, Almeida CN, Coelho VHR, Freitas ES, Galvão CO, Araújo JC. Sub-hourly rainfall patterns by hyetograph type under distinct climate conditions in Northeast of Brazil: a comparative inference of their key properties. Rev Bras Recur Hidricos. 2018;23:e46. https://doi.org/10.1590/2318-0331.231820180076

Brocca L, Ciabatta L, Massari C, Camici S, Tarpanelli A. Soil moisture for hydrological applications: open questions and new opportunities. Water. 2017;9:140. https://doi.org/10.3390/w9020140

Brocca L, Melone F, Moramarco T, Morbidelli R. Spatial-temporal variability of soil moisture and its estimation across scales. Water Resour Res. 2010;46:W02516. https://doi.org/10.1029/2009WR008016

Brocca L, Tullo T, Melone F, Moramarco T, Morbidelli R. Catchment scale soil moisture spatial-temporal variability. J Hydrol. 2012;422-423:63-75. https://doi.org/10.1016/j.jhydrol.2011.12.039

Brocca L, Zucco G, Mittelbach H, Moramarco T, Seneviratne SI. Absolute versus temporal anomaly and percent of saturation soil moisture spatial variability for six networks worldwide. Water Resour Res. 2014;50:5560-76. https://doi.org/10.1002/2014WR015684

Coelho VHR, Montenegro S, Almeida CN, Silva BB, Oliveira LM, Gusmão ACV, Freitas ES, Montenegro AAA. Alluvial groundwater recharge estimation in semi-arid environment using remotely sensed data. J Hydrol. 2017;548:1-15. https://doi.org/10.1016/j.jhydrol.2017.02.054

Coppola A, Comegna A, Dragonetti G, Lamaddalena N, Kader AM, Comegna V. Average moisture saturation effects on temporal stability of soil water spatial distribution at field scale. Soil Till Res. 2011;114:155-64. https://doi.org/10.1016/j.still.2011.04.009

Costa CAG, Araújo JC, Lopes JWB, Pinheiro EAR. Permanence of water effectiveness in the root zone of the Caatinga biome. Rev Caatinga. 2016;29:692-9. https://doi.org/10.1590/1983-21252016v29n320rc

Deza MM, Deza E. Encyclopedia of distances. Heidelberg: Springer; 2009.

Dias LCP, Macedo MN, Costa MH, Coe MT, Neill C. Effects of land cover change on evapotranspiration and streamflow of small catchments in the Upper Xingu River Basin, Central Brazil. J Hydrol: Reg Stud. 2015;4:108-22. https://doi.org/10.1016/j.ejrh.2015.05.010

Figueiredo JV, Araújo JC, Medeiros PHA, Costa AC. Runoff initiation in a preserved semiarid Caatinga small watershed, Northeastern Brazil. Hydrol Process. 2016;30:2390-400. https://doi.org/10.1002/hyp.10801

Gadelha AN, Coelho VHR, Xavier AC, Barbosa LR, Melo DCD, Xuan Y, Huffman GJ, Petersen WA, Petersen WA, Almeida CN. Grid box-level evaluation of IMERG over Brazil at various space and time scales. Atmos Res. 2019;218:231-44. https://doi.org/10.1016/j.atmosres.2018.12.001

Hang C, Nadeau DF, Jensen DD, Hoch SW, Pardyjak ER. Playa soil moisture and evaporation dynamics during the MATERHORN field program. Boundary-Layer Meteorol. 2016;159:521-38. https://doi.org/10.1007/s10546-015-0058-0

Hirschi M, Mueller B, Dorigo W, Seneviratne SI. Using remotely sensed soil moisture for land-atmosphere coupling diagnostics: the role of surface vs. root-zone soil moisture variability. Remote Sens Environ. 2014;154:246-52. https://doi.org/10.1016/j.rse.2014.08.030

Hu W, Chau HW, Qiu W, Si B. Environmental controls on the spatial variability of soil water dynamics in a small watershed. J Hydrol. 2017;551:47-55. https://doi.org/10.1016/j.jhydrol.2017.05.054

Huang X, Shi ZH, Zhu HD, Zhang HY, Ai L, Yin W. Soil moisture dynamics within soil profiles and associated environmental controls. Catena. 2016;136:189-96. https://doi.org/10.1016/j.catena.2015.01.014

IUSS Working Group WRB. World reference base for soil resources 2014, update 2015: International soil classification system for naming soils and creating legends for soil maps. Rome: Food and Agriculture Organization of the United Nations; 2015. (World Soil Resources Reports, 106).

Köppen W. Das geographische System der Klimate. In: Köppen W, Geiger G, editors. Handbuch der klimatologie. Berlin: Gebrüder Borntraeger; 1936. p. 1-44.

Li B, Rodell M. Spatial variability and its scale dependency of observed and modeled soil moisture over different climate regions. Hydrol Earth Syst Sci. 2013;17:1177-88. https://doi.org/10.5194/hess-17-1177-2013

Liu H, Zhao W, He Z, Liu J. Soil moisture dynamics across landscape types in an arid inland river basin of Northwest China. Hydrol Process. 2015;29:3328-41. https://doi.org/10.1002/hyp.10444

Liu YY, Evans JP, McCabe MF, de Jeu RAM, van Dijk AIJM, Su H. Influence of cracking clays on satellite estimated and model simulated soil moisture. Hydrol Earth Syst Sci. 2010;14:979-90. https://doi.org/10.5194/hess-14-979-2010

Melo RO, Montenegro AAA. Dinâmica temporal da umidade do solo em uma bacia hidrográfica no semiárido Pernambucano. Rev Bras Recur Hidricos. 2015;20:430-41. https://doi.org/10.21168/rbrh.v20n2.p430-441

Ministério da Agricultura - MA / Superintendência do Desenvolvimento do Nordeste - SUDENE. Levantamento exploratório - reconhecimento de solos do estado da Paraíba. Rio de Janeiro: Convênio de mapeamento de solos MA/EPE-SUDENE/DRN - Convênio MA/CONTAP/USAID/BRASIL; 1972. (Boletim Técnico, 15 - Série Pedologia, 8). Available from: http://library.wur.nl/isric/fulltext/isricu_i00003046_001.pdf

Mittelbach H, Seneviratne SI. A new perspective on the spatio-temporal variability of soil moisture: Temporal dynamics versus time-invariant contributions. Hydrol Earth Syst Sci. 2012;16:2169-79. https://doi.org/10.5194/hess-16-2169-2012

Molina AJ, Latron J, Rubio CM, Gallart F, Llorens P. Spatio-temporal variability of soil water content on the local scale in a Mediterranean mountain area (Vallcebre, North Eastern Spain). How different spatio-temporal scales reflect mean soil water content. J Hydrol. 2014;516:182-92. https://doi.org/10.1016/j.jhydrol.2014.01.040

Montenegro A, Ragab R. Hydrological response of a Brazilian semi-arid catchment to different land use and climate change scenarios: a modelling study. Hydrol Process. 2010;24:2705-23. https://doi.org/10.1002/hyp.7825

Montenegro AAA, Abrantes JRCB, Lima JLMP, Singh VP, Santos TEM. Impact of mulching on soil and water dynamics under intermittent simulated rainfall. Catena. 2013;109:139-49. https://doi.org/10.1016/j.catena.2013.03.018

Montenegro AAA, Ribeiro MR, Montenegro SMGL, Corrêa MM, Santos TEM. Potencialidades hídricas superficiais de Fernando de Noronha, PE, e alternativas para incremento da oferta. R Bras Eng Agric Ambiental. 2009;13:931-9. https://doi.org/10.1590/S1415-43662009000700016

Montenegro AAA, Souza TEMS, Souza ER, Montenegro SMGL. Temporal dynamics of soil moisture and rainfall erosivity in a tropical volcanic archipelago. J Hydrol. 2018;563:737-49. https://doi.org/10.1016/j.jhydrol.2018.06.047

Montenegro S, Ragab R. Impact of possible climate and land use changes in the semi arid regions: a case study from North Eastern Brazil. J Hydrol. 2012;434-435:55-68. https://doi.org/10.1016/j.jhydrol.2012.02.036

Nascimento NR, Fritsch E, Bueno GT, Bardy M, Grimaldi C, Melfi AJ. Podzolization as a deferralitization process: dynamics and chemistry of ground and surface waters in an Acrisol–Podzol sequence of the upper Amazon Basin. Eur J Soil Sci. 2008;59:911-24. https://doi.org/10.1111/j.1365-2389.2008.01049.x

Neris J, Jiménez C, Fuentes J, Morillas G, Tejedor M. Vegetation and land-use effects on soil properties and water infiltration of Andisols in Tenerife (Canary Islands, Spain). Catena. 2012;98:55-62. https://doi.org/10.1016/j.catena.2012.06.006

Ottoni MV, Ottoni Filho TB, Schaap MG, Lopes-Assad MLRC, Rotunno Filho OC. Hydrophysical database for Brazilian soils (HYBRAS) and pedotransfer functions for water retention. Vadose Zone J. 2018;17:170095. https://doi.org/10.2136/vzj2017.05.0095

Qiu Y, Fu B, Wang J, Chen L. Spatial variability of soil moisture content and its relation to environmental indices in a semi-arid gully catchment of the Loess Plateau, China. J Arid Environ. 2001;49:723-50. https://doi.org/10.1006/jare.2001.0828

Robinson DA, Campbell CS, Hopmans JW, Hornbuckle BK, Jones SB, Knight R, Ogden F, Selker J, Wendroth O. Soil moisture measurement for ecological and hydrological watershed-scale observatories: a review. Vadose Zone J. 2008;7:358-89. https://doi.org/10.2136/vzj2007.0143

Rosenbaum U, Bogena HR, Herbst M, Huisman JA, Peterson TJ, Weuthen A, Western AW, Vereecken H. Seasonal and event dynamics of spatial soil moisture patterns at the small catchment scale. Water Resour Res. 2012;48:W10544. https://doi.org/10.1029/2011WR011518

Rossato L, Angelis CF, Alvalá RCS. Impacto das características da superfície terrestre no algoritmo de inferência da umidade do solo no Brasil, utilizando observações do Sensor AMSR-E/Aqua. Rev Bras Recur Hidricos. 2013;18:137-56. https://doi.org/10.21168/rbrh.v18n4.p137-156

Rötzer K, Montzka C, Vereecken H. Spatio-temporal variability of global soil moisture products. J Hydrol. 2015;522:187-202. https://doi.org/10.1016/j.jhydrol.2014.12.038

Rozante JR, Vila DA, Chiquetto JB, Fernandes AA, Alvim DS. Evaluation of TRMM/GPM blended daily products over Brazil. Remote Sens. 2018;10:882. https://doi.org/10.3390/rs10060882

Sales EG, Almeida CN, Farias AS, Coelho VHR. Hydrodynamic characterization of soils within a representative watershed in northeast Brazil. Proc IAHS. 2014;364:94-9. https://doi.org/10.5194/piahs-364-94-2014

Santos CAG, Silva JFCBC, Silva RM. Caracterização hidrodinâmica dos solos da bacia experimental do Riacho Guaraíra utilizando o método Beerkan. Rev Bras Recur Hidricos. 2012;17:149-60. https://doi.org/10.21168/rbrh.v17n4.p149-160

Santos HG, Jacomine PKT, Anjos LHC, Oliveira VA, Lumbreras JF, Coelho MR, Almeida JA, Araújo Filho JC, Oliveira JB, Cunha TJF. Sistema brasileiro de classificação de solos. 5. ed. rev. ampl. [e-book]. Brasília, DF: Embrapa; 2018.

Silva JRL, Montenegro AAA, Monteiro ALN, Silva Junior VP. Modelagem da dinâmica de umidade do solo em diferentes condições de cobertura no semiárido pernambucano. Rev Bras Cien Agrar. 2015;10:293-303. https://doi.org/10.5039/agraria.v10i2a4219

Silva Junior VP, Montenegro AAA, Melo RO. Temporal stability of soil moisture in an experimental watershed in the Pernambuco semi-arid region. R Bras Eng Agric Ambiental. 2016;20:880-5. https://doi.org/10.1590/1807-1929/agriambi.v20n10p880-885

Silva TC, Silans AMBP, Paiva AED, Gadelha CLM, Pedrosa Filho LA, Andrade Filho LS, Santos JB, Camara ACF. Plano diretor de recursos hídricos da bacia do Rio Gramame. João Pessoa: Convênio SEMARH/SCIENTEC; 2000.

Souza ER, Montenegro AAA, Montenegro SMG, Matos JA. Temporal stability of soil moisture in irrigated carrot crops in Northeast Brazil. Agr Water Manage. 2011;99:26-32. https://doi.org/10.1016/j.agwat.2011.08.002

Sun F, Lü Y, Wang J, Hu J, Fu B. Soil moisture dynamics of typical ecosystems in response to precipitation: a monitoring-based analysis of hydrological service in the Qilian Mountains. Catena. 2015;129:63-75. https://doi.org/10.1016/j.catena.2015.03.001

Vachaud G, De Silans AP de, Balabanis P, Vauclin M. Temporal stability of spatially measured soil water probability density function. Soil Sci Soc Am J. 1985;49:822-8. https://doi.org/10.2136/sssaj1985.03615995004900040006x

Vereecken H, Huisman JA, Pachepsky Y, Montzka C, van der Kruk J, Bogena H, Weihermüller L, Herbst M, Martinez G, Vanderborght J. On the spatio-temporal dynamics of soil moisture at the field scale. J Hydrol. 2014;516:76-96. https://doi.org/10.1016/j.jhydrol.2013.11.061

Viola F, Daly E, Vico G, Cannarozzo M, Porporato A. Transient soil-moisture dynamics and climate change in Mediterranean ecosystems. Water Resour Res. 2008;44:W11412. https://doi.org/10.1029/2007WR006371

Ward Jr JH. Hierarchical grouping to optimize an objective function. J Am Stat Assoc. 1963;58:236-44. https://doi.org/10.1080/01621459.1963.10500845

Weisheimer A, Doblas-Reyes FJ, Jung T, Palmer TN. On the predictability of the extreme summer 2003 over Europe. Geophys Res Lett. 2011;38:L05704. https://doi.org/10.1029/2010GL046455

Zhang S, Shao M. Temporal stability of soil moisture in an oasis of northwestern China. Hydrol Process. 2017;31:2725-36. https://doi.org/10.1002/hyp.11200

Zhao L, Yang K, Qin J, Chen Y, Tang W, Montzka C, Wu H, Lin C, Han M, Vereecken H. Spatiotemporal analysis of soil moisture observations within a Tibetan mesoscale area and its implication to regional soil moisture measurements. J Hydrol. 2013;482:92-104. https://doi.org/10.1016/j.jhydrol.2012.12.033

Zhou J, Fu B, Gao G, Lü N, Lü Y, Wang S. Temporal stability of surface soil moisture of different vegetation types in the Loess Plateau of China. Catena. 2015;128:1-15. https://doi.org/10.1016/j.catena.2015.01.015

Zhu HD, Shi ZH, Fang NF, Wu GL, Guo ZL, Zhang Y. Soil moisture response to environmental factors following precipitation events in a small catchment. Catena. 2014;120:73-80. https://doi.org/10.1016/j.catena.2014.04.003

Revista Brasileira de Ciência do Solo

In the article “Stability of Soil Moisture Patterns Retrieved at Different Temporal Resolutions in a Tropical Watershed” [Rev Bras Cienc Solo. 2019;43:e0180236. DOI: 10.1590/18069657rbcs20180236], on page 13 (Figure 5) and 15 (Figure 7), where it is presented:

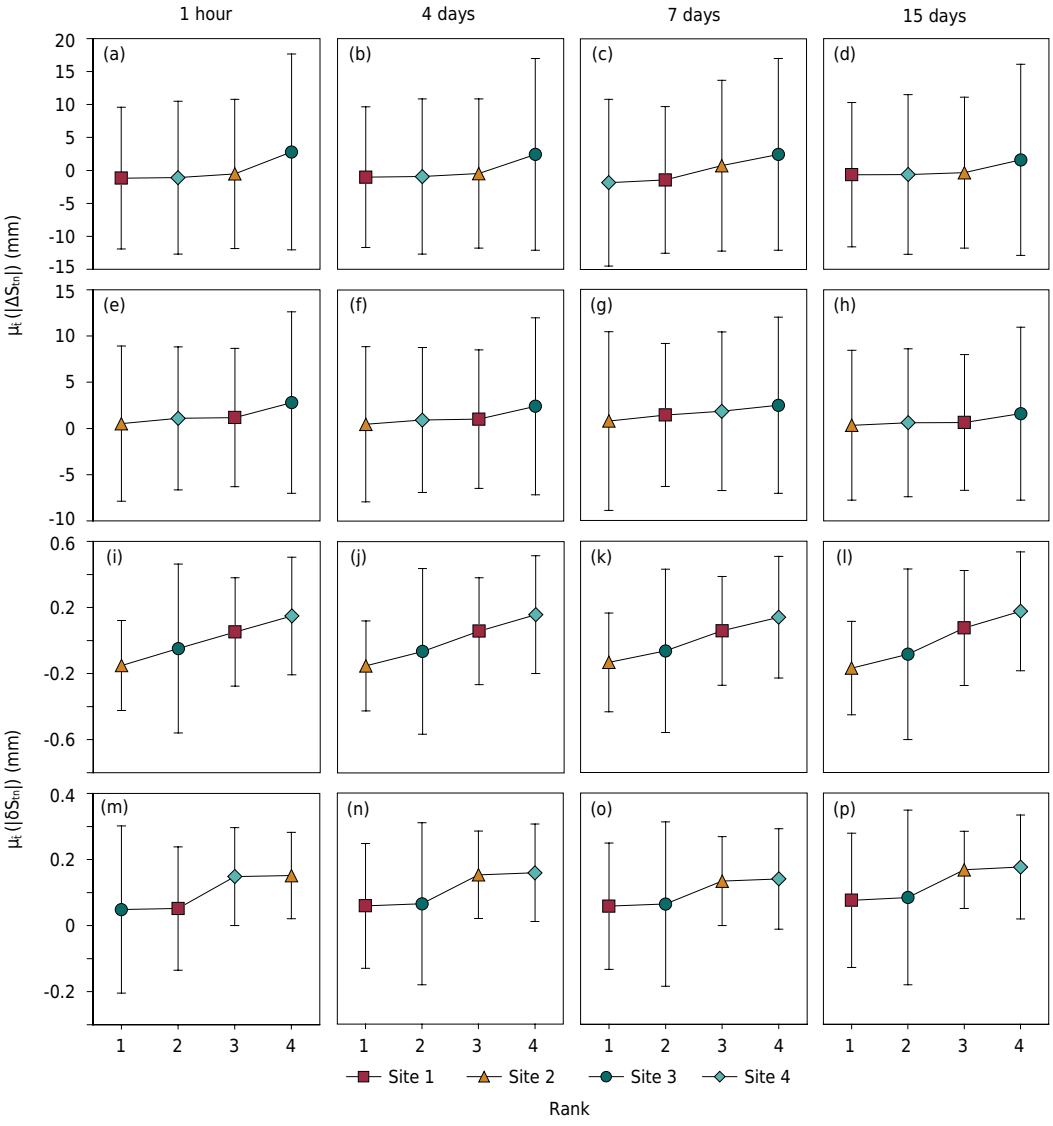

Figure 5. Ranking stability plots of temporal means of absolute Soil Moisture (SM) differences [$\mu_t(\Delta S_{tn})$] (a, b, c, and d), absolute temporal means of absolute SM differences [$|\mu_t(\Delta S_{tn})|$] (e, f, g), and temporal means of relative SM differences [$\mu_t(\delta S_{tn})$] and absolute temporal means of relative SM differences [$|\mu_t(\delta S_{tn})|$] (i, j, k, and l).

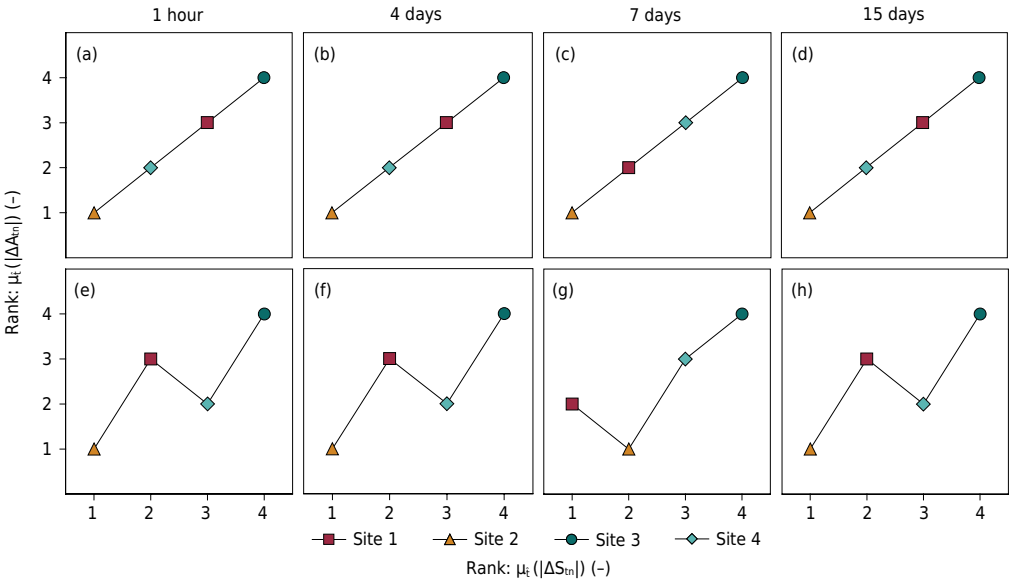

Figure 7. Scatter plots of absolute temporal mean ranking of absolute soil moisture differences [$|\mu_t(\Delta S_{tn})|$] against the temporal mean ranking of absolute SM temporal mean differences $\mu_t(|\Delta M_{tn}|)$ (a, b, c, and d) and temporal mean ranking of absolute temporal anomaly differences $\mu_t(|\Delta A_{tn}|)$ (e, f, g, and h).

It should be presented:

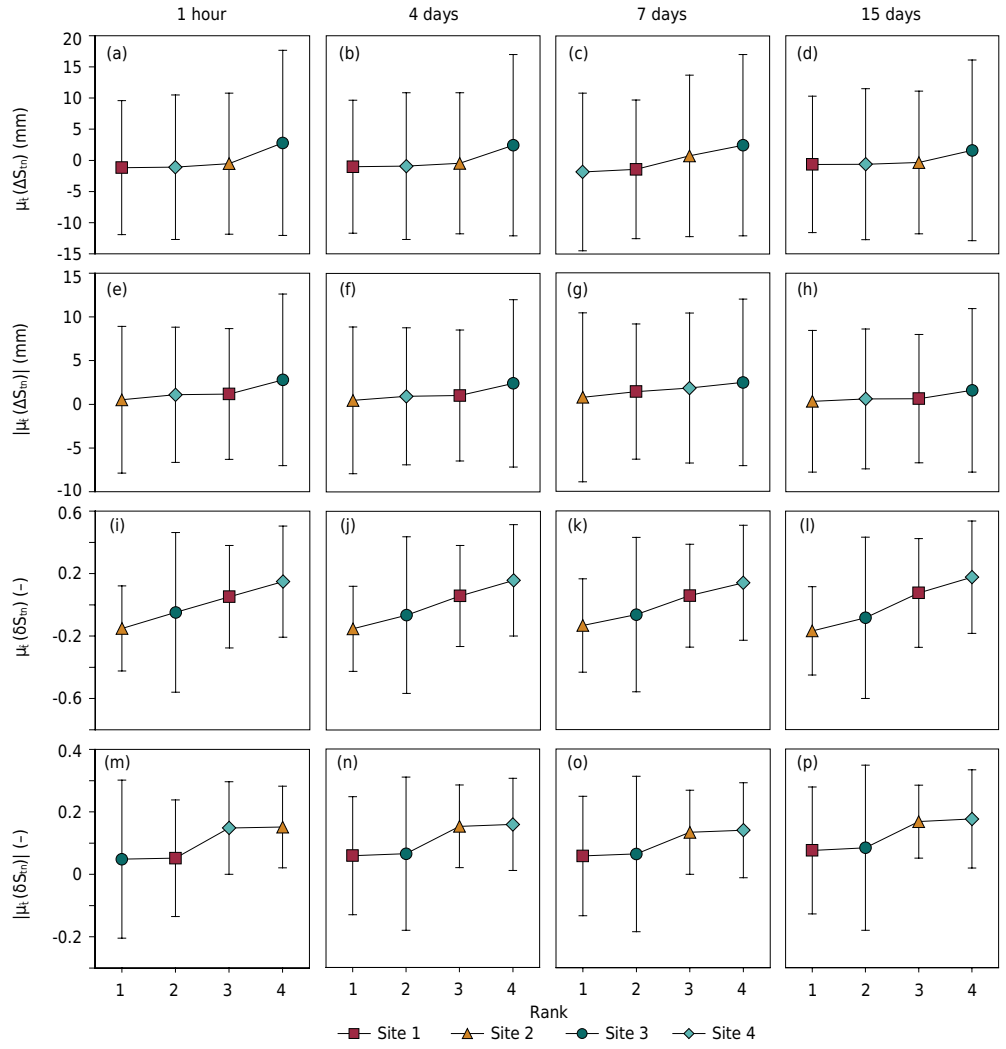

Figure 5. Ranking stability plots of temporal means of absolute Soil Moisture (SM) differences [$\mu_t(\Delta S_{tn})$] (a, b, c, and d), absolute temporal means of absolute SM differences [$|\mu_t(\Delta S_{tn})|$] (e, f, g, and h), temporal means of relative SM differences [$\mu_t(\delta S_{tn})$] (i, j, k, and l), and absolute temporal means of relative SM differences [$|\mu_t(\delta S_{tn})|$] (m, n, o, and p).

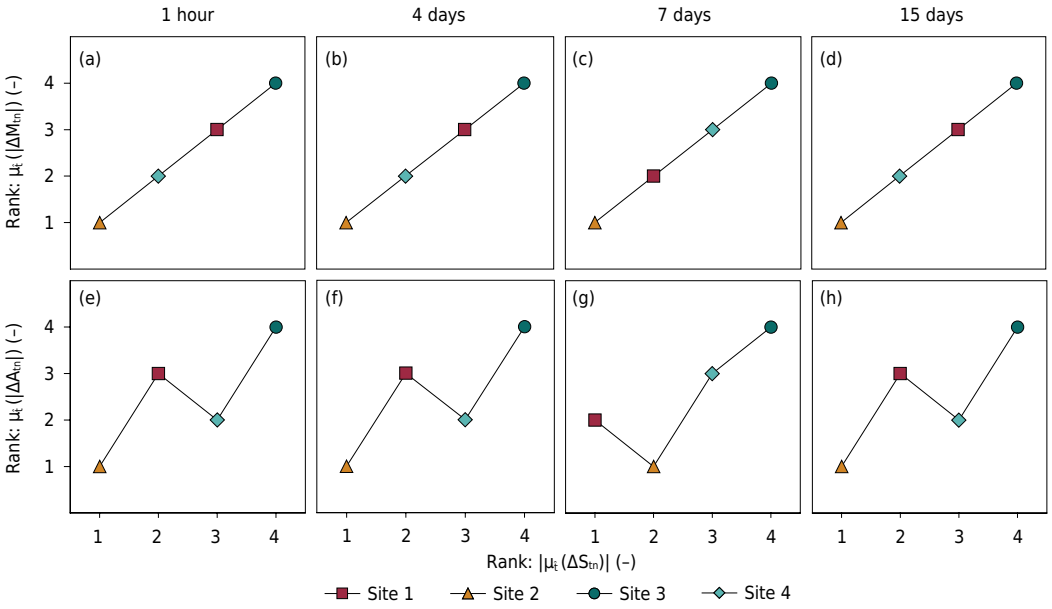

Figure 7. Scatter plots of absolute temporal mean ranking of absolute Soil Moisture (SM) differences [$|\mu_t(\Delta S_{tn})|$] against the temporal mean ranking of absolute SM temporal mean differences [$\mu_t(|\Delta M_{tn}|)$] (a, b, c, and d) and temporal mean ranking of absolute SM temporal anomaly differences [$\mu_t(|\Delta A_{tn}|)$] (e, f, g, and h).